Forward Osmosis for the Treatment of Oil Sands Produced Water

by

Amrit Pal Singh Bhinder

A thesis submitted in partial fulfillment of the requirements for the degree of

Master of Science

Department of Mechanical Engineering
University of Alberta

© Amrit Pal Singh Bhinder, 2015

Abstract

Forward osmosis (FO) technology has attracted a lot of attention in the last decade due to its promising future to provide clean water and energy. In this study the feasibility of FO was studied for treatment of SAGD produced water. First, the effects of temperature, flow rate and pH of the feed water as well as concentration and flow rate of the draw solution (salt solution) on the water flux were studied using Taguchi design of experiment. It was found that increasing the feed temperature and the draw solution concentration enhanced the water flux. The change in feed pH didn't have any significant affect on water flux. Increasing the flow rate of both the feed and the draw solution reduced the concentration polarization layer on both sides, thus increasing the efficiency of the separation process.

In the second part of this study, previously existing models for FO were modified by incorporating new mass transfer coefficients and the applicability of the model for prediction of the produced water treatment was verified. Experimental investigations were made through reverse osmosis (RO) and pressure retarded osmosis (PRO) to estimate the value of mass transfer coefficient. Using the new mass transfer coefficients has overcome the main shortcoming of previous models which were insensitive to the feed flow rate. It was also shown that theoretical model with the modified values of the mass transfer coefficient predicted the performance of FO reasonably when SAGD produced water with moderate concentration of salt and organic matter was used as the feed solution.

The last part of this work demonstrates the fabrication of high performance thin film composite (TFC) membrane for FO applications. The polyamide (PA) TFC membranes were synthesized by interfacial polymerization (IP) reaction between two monomers dissolved in two immiscible solvents (organic and aqueous) at the surface of a microporous support. Three membranes were fabricated at different temperatures (-20˚C, 1˚C and 25˚C) of the organic solution. The membranes prepared at -20˚C had the thinnest active layer and provided the highest water flux (39.5 LMH) using 3 M NaCl solution as draw solution and DI water as feed. Comparing the performance of these membranes with commercial TFC membranes, it is found that lab fabricated membranes provided higher permeation and rejection than the commercial membrane.

Preface

This thesis highlights the first applications of FO for the treatment of *in-situ* SAGD produced water. Chapter 2 of this thesis "Forward osmosis for treatment of oil sands produced water: Systematic study of influential parameters" has been submitted to *Desalination and Water Treatment* Journal. This work has also been presented in EuroMed 2015 *Desalination for Clean Water and Energy* conference and 2015 *Faculty of Engineering Graduate Research Symposium* (FEGRS). It was awarded the best poster in Engineering for a Sustainable Future session in FEGRS.

Chapter 3 entitled "Modeling of FO process: Experimental investigation of mass transfer coefficient" has been prepared for submission to *Separation and Purification Technology Journal*. Chapter 4, "Ultra thin film composite membrane for FO process" has been submitted to the *Journal of Membrane Science.* I am the first author of the first two papers and the second author in the last one. The last study was a collaborative work and I helped to identify the scope of the work, conducted FO experiments and analyzed the results.

Acknowledgement

I am using this opportunity to express my profound gratitude and regards to my supervisor Dr Mohtada Sadrzadeh. He has been an excellent mentor and it was only through his support and guidance that I am able to achieve this goal. I am highly thankful to him for the amount of time he has spent in answering my questions and giving valuable suggestion on improving my troubleshooting skills, engineering aptitude and guidance on carrying out research experiments that helped me to successfully accomplish my degree program's objectives (to become an expert learner).

I would like to thank my fellow colleagues Behnam Khorshidi and Hadi Nazaripoor for being so helpful, to me whether it was regarding troubleshooting an experiment, writing a paper or be any general piece of advice you guys were always there. Thanks once again.

I would also acknowledge my friends Chunendra Sahu, Pankaj Sahu, Sourayon Chanda, Alexey Baldygin, Abdul Wasay, Swayamdipt Bahaduri, Debal Saha and others for helping me at numerous occasions and making my stay in Edmonton enjoyable. Last, but no way the least, I would like to thank my dearest friend Mersedeh Zandvakili for always being there with me. And finally I would also not miss this opportunity to thank my parents for their love, support and endless faith in me.

TABLE OF CONTENTS

LIST OF TABLES

LIST OF FIGURES

LIST OF NOMENCLATURE

Abbreviations

BBD	Boiler Blow Down
BFW	Boiler Feed Water
CP	Concentration Polarization
DOM	Dissolved Organic Matter
ECP	External Concentration Polarization
FO	Forward Osmosis
ICP	Internal Concentration Polarization
ISF	Induced Static Floatation
MD	Membrane Distillation
MF	Microfiltration
NF	Nanofiltration
OSPW	Oil Sands Process Affected Water
O&G	Oil and Gas
OTSG	Once Through Steam Generator
PA	Polyamide
PSf	Polysulfone
PES	Polyethersulfone
RO	Reverse Osmosis
SAGD	Steam Assisted Gravity Drainage
SS	Sum of squares
TFC	Thin Film Composite
TOC	Total Organic Carbon
TDS	Total dissolved Solids
UF	Ultrafiltration
WAC	Weak Cationic Exchanger

Symbols

A	pure water permeability (LMH/atm)
B	solute permeability (LMH)
c	concentration of solute (mol/L)
d_h	hydraulic diameter (m)
D	diffusion coefficeint (m^2/s)
F	F statistics
i	Van't Hoff factor
J	flux (LMH)
k	mass transfer coefficent (m/s)
K	solute resistivity in the support layer of membrane (s/m), number of levels of a particular factor
L	length of channel (m)
n	number of observations at level i
N	number of observations
P	hydraulic pressure (atm), percentage influence of a factor
R_g	real gas constant(L atm/ (mol K))
R_j	salt rejection
R_m	intrinsic hydraulic resistance
Re	Reynolds number
Re_L	Reynolds number at L
Re_t	transition Reynolds number
Sc	Schmidt number
Sh	Sherwood number
S	Structural parameter (μm)
T	absolute temperature (K), total sum of all observations
V	Variance
v	cross flow velocity (m/s)

Greek symbols

δ	thickness of external concentration polarization boundary layer (m)
α	Risks
ε	porosity of membrane support
μ	dynamic viscosity (m^2/s)
ν	degree of freedeom
ρ	density of water (kg/m^3)
τ	tortuosity of membrane support
π	osmotic pressure (atm)

Subscripts

A, B	factors A and B
b	bulk solution
D	draw solution
e	Error
F	feed solution
i	interaface between support layer and active layer of membrane, level of factor
m	membrane surface
s	solute
T	total
v	pure water
w	water

CHAPTER 1: INTRODUCTION

1.1 Background and Overview

Since the beginning of time, the advancement of human race has always thrived on the availability of freshwater. All the known ancient human civilizations settled in the river valleys and on the flood plains. Not only to the humans, but water is also the key component to all forms of lives on earth. Though water covers about 75% of our planet's surface, only 2.5% is fresh water and two-third of this small percentage is frozen in glaciers and ice caps. So, less than 1% of all the fresh water on our planet is available to us from rivers, lakes and underground water [1].

Exponential growth and rapid industrialization has not only caused an increase in the demand of freshwater supply but has also caused the pollution of the existing freshwater resources resulting in its depletion and creating a scarcity of water globally. It is reported that around 1.2 billion people across the globe have limited access to clean water and these figures are expected to rise in the near future [2–4]. Furthermore, the decline in quantity and quality of water has not only affected human society but has also resulted in disruption of the natural ecological system. The climate change has added fuel to the fire by bringing changes in the weather pattern causing erratic draughts and variable monsoon pattern thus affecting the timing and volume of flow in rivers and the height of ground water table [5]. So to deal with the upcoming crisis of water scarcity, the management of water resources has become critical for sustainable development. Water management should not only aim at conservation of existing freshwater resources but should also push forward new ways to increase the supply of fresh water to meet the growing demand in future. With finite freshwater resources on our planet, the only viable options to sustainable economic growth are desalination of seawater and reclamation of wastewater.

Desalination technologies have the potential to provide an unlimited supply of freshwater from seawater [6]. Several desalination plants have been installed in the arid Persian Gulf countries and in the Mediterranean region to meet the demand for freshwater supply. The global freshwater supply by desalination plants is projected to exceed 38 billion m^3 per year by 2016 which is double the rate of its production in 2008 [6]. But for the countries located inland or places far away from the coast, the construction of desalination plants is not a feasible option. So, water reclamation and recycling is one of the ways these regions can address their demand for freshwater without putting much pressure on the available freshwater resources. However, according to the water-energy nexus, generation of clean water and its distribution requires energy and energy generation needs water [7]. Desalination and all the known wastewater reclamation processes are energy intensive processes. Most of the energy required is either in the form of electrical energy or thermal energy which comes from burning fossil fuels. On the other hand, almost all sources of energy production require water in one stage of production process or the other like thermal and nuclear power plants require an enormous quantity of water for cooling and fuel processing. In oil and natural gas industry water is key commodity for drilling and extraction purposes, e.g. oil sands and shale gas industries require water for *in-situ* extraction processes, processing, waste disposal and land reclamation [8]. Meeting the demand for clean water by using conventional energy sources will only add to our problems causing severe impacts on the environment. Hence, there is not only a need to put a check on our water consumption but also alternative sources of clean energy need to be explored so that the need for clean water and energy can be met in a sustainable way.

One of the industries which is highly dependent on water usage is the Canadian oil sands industry [9]. The extraction process of bitumen from the oil sands can either be done through open pit mining or through *in-situ* processes. Mining operation can only be performed on shallow bitumen deposits which lie close to the surface but about 80% of the bitumen deposits are not accessible through mining activity [10]. So, *in-situ* methods are being employed for the recovery of these deposits. Water is the driver of thermally enhanced *in-situ* processes, called steam assisted gravity drainage (SAGD), as they

require steam to be injected underground to assist in the extraction of bitumen. As shown in Fig. 1.1, in this process, two parallel wells are drilled horizontally underground, one above the other and the top well (injection well) is flooded with saturated steam causing the bitumen to melt and accumulate in the bottom well (production well). This melted bitumen along with steam condensate is then pumped up to the surface through production well, where water is separated from the bitumen and recycled to be used as boiler feed water (BFW).

The required water for the SAGD operation is typically obtained from local rivers and underground water tables. With the continuous growth in the oil sand industries the consumption of water from the local rivers has increased significantly which has alarmed the environmental activists. Hence, in order to keep a balance of the river ecological system, the withdrawal of water from the local rivers has been controlled and limited to a maximum of 3% of the annual river flow. According to some studies even this amount can cause damage to the river ecosystem [9]. In addition to the risk of depletion of fresh water, the disposal of wastewater by the current practices results in polluting the river and groundwater posing a threat to the surrounding flora and fauna [9,11]. Therefore, there is huge pressure on the oil sands industries to seek alternative produced water treatment methods to minimize the freshwater usage and to recycle as water much as possible.

The produced water in the SAGD process is treated in two steps: (i) separation of bitumen from water and (ii) water treatment, the latter is the focus of our study. The separated water from bitumen is first de-oiled by passing it through gravity skim tanks followed by induced static floatation (ISF) and walnut shell filters bringing the oil content to below 20 mg/L. After de-oiling, the produced water is passed through the warm lime softener (WLS) to remove silica, then through after-filters to remove suspended solids and finally through weak-acid cation exchangers (WAC) to remove the left over Ca^{+2} and Mg^{+2} ions. This treated water is then fed into the steam generators to generate steam. Once through steam generators (OTSG) are the most common types of boilers used in the SAGD process as they are more robust and can operate with low

quality of feed having high level of total dissolved solids (TDS) (< 8000 ppm) than the conventional drum boilers [12].

The water after the conventional treatment has high level of TDS and silica, which limits the operation of OTSG's to a steam quality of 75 to 80% [13]. Operation in this range ensures that sufficient water volume wets the inner wall tube so that the impurities in BFW remain dissolved in the liquid phase and are not deposited on the tube surface. At the exit, the quality of steam is increased by a vapor-liquid separator and is then sent into injection wells. The separated liquid has high concentration of TDS and dissolved organics and is known as boiler blowdown water (BBD). A part of BBD is recycled to be fed in WLS while the rest is disposed off.

The low quality of BFW with high amount of TDS, silica and dissolved organic matter (DOM) has increased the vulnerability of boiler tubes to fouling resulting in the decreased efficiency of heat exchanger, additional maintenance cost to remove fouling deposits and also premature failure of boiler tubes leading to a loss in productivity [13–15]. Lower feed water quality also results in high blow down volumes (about 20% of BFW) [16] from the OTSGs requiring more make up water to compensate for the poor quality of recycled water. Hence, to address these problems of current technology, the oil sands industries are seeking alternative water treatment processes that can provide high quality feed water with low concentration of TDS, organics and silica. A plausible solution to this problem can be achieved by replacing the conventional treatment process with a membrane based separation process. Membranes have been highly efficient in treating municipal as well as industrial wastewaters. Microfiltration (MF) and ultrafiltration (UF) processes have been applied for removing oil from oily wastewaters [17–22] while tighter membrane based separation processes like reverse osmosis (RO) and nanofiltration (NF) have been applied for treatment of silica, dissolved solids and organic matter in the produced water [23–31]. These studies showed effectiveness of the membrane based separation processes in treating contaminated water produced from various sources during oil extraction operations.

As we move towards a more sustainable future, we need to evolve processes with lesser energy consumption. Though pressure driven membrane processes (RO and NF) provide high rejection, the amount of energy required to drive these processes may limit their application in the near future. In the search for processes with lower energy consumption, one of the membrane processes which have been introduced as a viable solution is the forward osmosis (FO) process. FO is an emerging membrane technology which has the potential to solve the global crisis of energy and water. It utilizes the natural osmotic pressure difference between the two solutions to drive the flow through a semi permeable membrane allowing solvent molecules to pass through it while retaining the solute molecules. The driving force is provided by the osmotic potential difference between a concentrated solution known as "draw" solution and the less concentrated solution known as "feed" solution. The feed solution is generally the impaired water from which the dissolved solids and contaminants has to be removed. Another important fact about this process is that it can be used to generate energy by harnessing the osmotic gradient through hydraulic pressure and generating useful work. This process is known as pressure retarded osmosis (PRO). PRO has the potential to capture the energy from nature, i.e. areas where river water meets the sea and also from existing desalination plants which dispose concentrated brine into the sea. Energy obtained from PRO process is termed as "blue" energy as it is renewable and have negligible carbon footprint [4]. Researchers have estimated that full fledge PRO operations across the globe have a potential to provide 2000 TWh of energy per year. But currently, due to the lack of high performance and low cost membranes, PRO is not able to provide energy at a reasonable cost [32].

In the past decade, researchers have shown the feasibility of FO in various fields of wastewater treatment [33], desalination [34,35] and power generation [32,36]. The popularity of the FO, as mentioned above, lies in the fact that it requires minimal or no hydraulic pressure for recovery of water as shown in Fig. 1.2, thus saving substantial amount of energy, providing it an edge over existing pressure driven processes [33]. However, this process also uses some amount of energy for the regeneration of the draw solution [37]. Eliminating the use to hydraulic pressure gives another advantage to FO

over pressure driven process which includes minimal treatment of feed and less membrane fouling [38,39] ensuring longer operations with the same membrane thus reducing maintenance cost.

1.2 Theoretical Background

A membrane can be described as a barrier which selectivity allows one component to pass through while retains the other. The theory of mass transport across the membrane is based on the thermodynamics principles, i.e. the movement of molecules across the membrane is due to its chemical potential difference. The chemical potential gradient inter-relates all the driving forces of pressure, concentration and temperature difference. The flux of a component is thus proportional to the chemical potential gradient and is expressed as:

$$J_i = -L_i \frac{\mathrm{d}\mu_i}{\mathrm{d}l} \tag{1.1}$$

Where $d\mu_i/dl$ is the chemical potential gradient across membrane of thickness l and L_i is a proportionality coefficient. Generally, under isothermal condition the chemical potential can be expressed as a function of pressure and concentration. If we assume that the chemical potential gradient is only a function of concentration gradient inside the membrane then the above model is termed as solution-diffusion model and if the chemical potential is represented only as a function of pressure gradient across the membrane then it is termed as pore-flow model [40]. In the pore flow model it is assumed that the flow through the membrane occurs through micro porous channel by convection and separation is achieved when solute molecule is blocked by some of the pores in the membrane. Applying the assumption of no concentration gradient across the membrane in Equation 1.1 gives us Equation 1.2 which is Darcy's law for flow in porous media:

$$J_i = -K' c_i \frac{\mathrm{d}p}{\mathrm{d}x} \tag{1.2}$$

Here dp/dx is the pressure gradient across the membrane, K' is a coefficient representing nature of medium and c_i is concentration of component i.

In the solution-diffusion model, the transportation of solvent across the membrane occurs by diffusion along the concentration gradient and the separation is achieved due the difference in the solubility and rate of diffusion of the solute and the solvent in the membrane. So, in the absence of pressure gradient, Equation 1.1 gives the following equation which is the Fick's law of diffusion:

$$J_i = -D_i \frac{\mathrm{d}c_i}{\mathrm{d}x} \tag{1.3}$$

where D_i is diffusion coefficient and dc_i/dx represents the concentration gradient of component i across the membrane [40]. The solution-diffusion model is best used to describe the flow through the membranes which are very dense and tight like the membranes used in RO and FO. These membranes virtually have no pores and the available space for movement of solvent is at molecular level. While the flow through MF and UF membranes are best described by the pore flow model. These membranes have real interconnected pores acting like channels for the solvent to pass through. Generally pore flow is dominant in membranes which have pores larger than 10-15 Å while for the solution diffusion model to apply, the available space for the movement of permeate should be in the range of 2-5 Å [41].

Solution-diffusion model is commonly used to describe the transport phenomena in a RO process. Chemical potential in a RO process is dependent on both concentration and pressure gradients. So applying the assumptions of the solution-diffusion model we get a simplified equation:

$$J_{\mathrm{w}} = A(\Delta\pi - \Delta P) \tag{1.4}$$

where $\Delta P > 0$, J_{w} is the water flux through the membrane, A is the pure water permeability of the membrane. A is an intrinsic property of a membrane and determines

the ease of diffusion of water molecules through the membrane or in other words it represents the resistivity of membrane to the passage of pure water.

In a RO process, hydraulic pressure is applied against the osmotic pressure gradient to drive the flow of permeate through the membrane. If there is no hydraulic pressure, then the movement of permeates can be facilitated by creating a difference in the osmotic pressure of the two solutions, which is the idea behind the FO process. In absence of applied hydraulic pressure ($\Delta P = 0$), the flux equation can be represented as the osmotic pressure difference between the two solutions:

$$J_w = A\Delta\pi = A(\pi_{\mathrm{D}} - \pi_{\mathrm{F}}) \tag{1.5}$$

where π_{D} the osmotic pressure of the concentrated draw solution and π_{F} is the osmotic pressure of the less concentrated feed solution. In a PRO process the applied hydraulic pressure is less than the osmotic pressure i.e. $\Delta P < 0$ [33]. Fig. 1.3 shows the magnitude and direction of water flux with the applied hydraulic pressure for a FO, PRO and RO process.

Another important parameter that is used to evaluate the membrane performance is its rejection, i.e. its capability to separate the solute from the solution. This is judged by the retention or rejection coefficient of a membrane which is given by:

$$R_j = \left(1 - \frac{c_{\mathrm{p}}}{c_{\mathrm{F}}}\right) \times 100 \tag{1.6}$$

where c_{p} is the concentration of solute in the permeate and c_{F} is the concentration of the solute in the feed. Ideally for a perfect membrane, the rejection coefficient (R_j) should be 100% i.e. membrane is able to retain all the solute.

1.3 Literature Review

Here we present a literature survey on application of FO for Oil and Gas (O&G) produced water treatment. Produced water is the contaminated water which is brought to

the surface during extraction of O&G or the water which is contaminated by the earthly matter while being used in exploration and drilling of unconventional oil [42]. Hence, produced water is mainly composed of organic and inorganic compounds and its composition may vary depending upon the site of extraction and the process and chemicals used for extraction [42].

Based on the type of contaminant to be rejected, different membranes processes are used. UF has been found to very effective in treatment of oily wastewater and suspended solids [17,21,43]. While tighter like NF and RO membranes are used for removing dissolved solid and metal ions from impaired water [23,28,42]. But RO and NF are highly susceptible to choking of the membranes by particulate matter present in the wastewater leading to lower fluxes and higher energy consumptions [44]. Till now there have been very limited applications of these systems in treating produced water and very few studies are available in the literature showing their applicability in treating oil and gas produced water [23–31,45].

FO is an emerging technology which has a high potential to be applied in wastewater treatment. FO membrane can achieve rejection rate of almost all solutes and dissolved organics [46]. Also FO membranes are less susceptible to fouling [47]. Moreover, FO can be setup as independent portable and can be used in locations with limited access to external power source [44]. With these inherent advantages, FO has found application in various fields of wastewater treatment and desalination either as a pre-treatment of process to other membrane operations like RO, NF and MD or as an independent process where draw solution gets diluted with time and is used for other purposes [48–51]. Areas of application of FO include seawater desalination [34,52], treatment of landfill leachates [53], concentration of sludge [39,54] and industrial wastewater [55,56]. Although a few studies have been conducted on application of FO in oilfield produced water treatment, to the best of our knowledge, FO has never been used for treatment oil sands produced water.

Hutching et al. [50] evaluated the performance of FO on the wastewater generated during exploration and production of shale gas. The wastewater was particularly generated during the hydraulic fracturing of the formations to extract shale gas. A movable and scalable pilot testing system was developed so that onsite treatment of wastewater was possible. The pilot system used 26% w/w NaCl as the draw solution and was operated in osmotic dilution mode till the draw solution was diluted to around 7% w/w of NaCl. A recovery of more than 70% of water from a typical wastewater pit was observed and the concentration of barium, calcium and other heavy metals was significantly reduced. This diluted draw was reused for the further drilling operation. With promising results from the pilot scale experiments, this FO system was setup on a commercial scale by Bear Creek Services and HTI and was named the Green Machine. This Green Machine was able to provide approximately 12% of the needs of total water requirement for hydraulic fracturing in Haynesville Shale well.

Later, Hickenbottem et al. [57] conducted another study to further optimize the performance of The Green Machine. Bench scale experiments were performed to treat drilling wastewater obtained from Northern Louisiana shale gas fields with commercial HTI cellulose triacetate (CTA) membranes using a draw solution of 26% w/w NaCl. Results showed that FO process was able to recover more than 80% water from the wastewater stream. Operations at high cross flow velocities increased water flux through the membrane by decreasing membrane fouling and concentration polarization. Initial flux through the membrane was restored by osmotic backwashing technique showing that the fouling was reversible in nature. Moreover, FO membrane showed a high rejection against organics as well as inorganic compounds proving the effectiveness of FO in treating drilling wastewater.

Another study was conducted by Coday et al. [58] to investigate the performance of FO on treating produced water obtained from Niobrara Shale gas field. Three different types of commercial membranes obtained from HTI (CTA and 2 different TFC) were tested under operating conditions similar to the one practiced in industrial FO process (i.e. spiral

wound modules). It was reported that in short term, fouling was mainly affected by initial decline in water flux and the permeate drag force but in long term, i.e. after the formation of cake layer, foulant-foulant interactions were responsible for the fouling for all types of membranes. High rejection of inorganic and organic compounds was achieved showing that spiral wound FO setup can be applied to treat the oil and gas waste streams.

1.4 Objectives

The main goals of this thesis are (i) to study the effectiveness of the FO process in treatment of SAGD produced water, (ii) to develop a predictive FO model for real produced water, and (iii) synthesis of thin film composite (TFC) membranes with comparable permeation properties as commercial membranes for FO. This was achieved by getting a better understanding of the process both through experimental and theoretical results. The main objective of this thesis was met by conducting study in three phases as discussed below:

- In the first phase of this study the effectiveness of FO in treating an *in-situ* produced water stream obtained from SAGD operation (BFW) was studied for removal of DOM using commercially available TFC membranes. The effect of influential parameters like feed temperature and pH, draw solution concentration, feed flow rate and draw flow rate on water flux was also investigated by using Taguchi design of experiment.
- In the second phase, modeling of the FO process was done to predict its performance for real *in-situ* oil sands produced water as feed at different operating conditions. Experimental techniques were suggested to estimate the values of mass transfer coefficient in a FO process.
- In the third phase, the objective was to test and compare the performance of lab fabricated TFC membranes with commercial TFC membranes obtained from HTI technology. The water flux and DOM rejection of these membranes are compared for SAGD produced water filtration.

1.5 Thesis Outline

Chapter 1 of the thesis gives a brief idea about the SAGD process and the conventional produced water treatment technology used by the oil sands industries. The limitations of the current water treatment technology are discussed and membrane based separation processes are presented as possible solution to these limitation. Among the membrane based separation process, FO is introduced as a future alternative to the current pressure driven membrane based separation processes due to its lower energy consumption and ability to treat high salinity feed solution. Following which the principle of forward osmosis and its potential to provide clean water and energy (PRO process) is discussed. Different models governing the flow through membranes are discussed and the flux equation for FO was established through these models. At the end of this chapter a literature review on application of FO for treatment of oilfield produced water has been presented.

In the second chapter of the thesis the applicability of forward osmosis to treat the SAGD produced was studied for the first time. The effect of various influential parameters like feed temperature, draw solution concentration, draw and feed flow rate and feed pH on water flux and rejection of total organic carbon (TOC) was investigated using the Taguchi design of experiment. Finally, the performance of the FO process was optimized in terms of water flux.

In the third chapter, an attempt was made to better understand the FO process by modeling the flow through the FO membrane. In this study it was shown that using the value of mass transfer coefficient derived from Sherwood number relations, which were developed for UF experiments, may not be viable for a FO process. The values of mass transfer coefficients were determined experimentally by two methods (i) RO and (ii) PRO experiments. The values of mass transfer coefficient found from these experiments were found to be an order of magnitude less than the theoretical values of the mass transfer coefficient obtained from Sherwood number correlations. In the latter part of the study it was shown that theoretical model with modified values of the mass transfer coefficient

can be used to predict the performance of the FO at different operating conditions when less concentrated produced water was used as the feed solution.

In Chapter 4, due to the limited performance of the commercial TFC membrane, particularly water flux, we fabricated and tested the performance of our self-synthesized TFC membranes. The lab fabricated TFC membranes were made based on a novel idea of lowering the temperature of the organic solution in the polymerization reaction of two monomers dissolved in two immiscible solvents (organic and aqueous). Ultra-thin film of Polyamide (PA) on the polyethersulfone (PES) support interface was synthesized. It was shown that lab fabricated TFC membranes were less prone to internal concentration polarization and achieved three times higher fluxes than the commercial membrane while maintaining comparable rejection rates.

In Chapter 5 the major findings of this work has been summarized. Based on the outcome of this work, recommendations are provided for further development in this field.

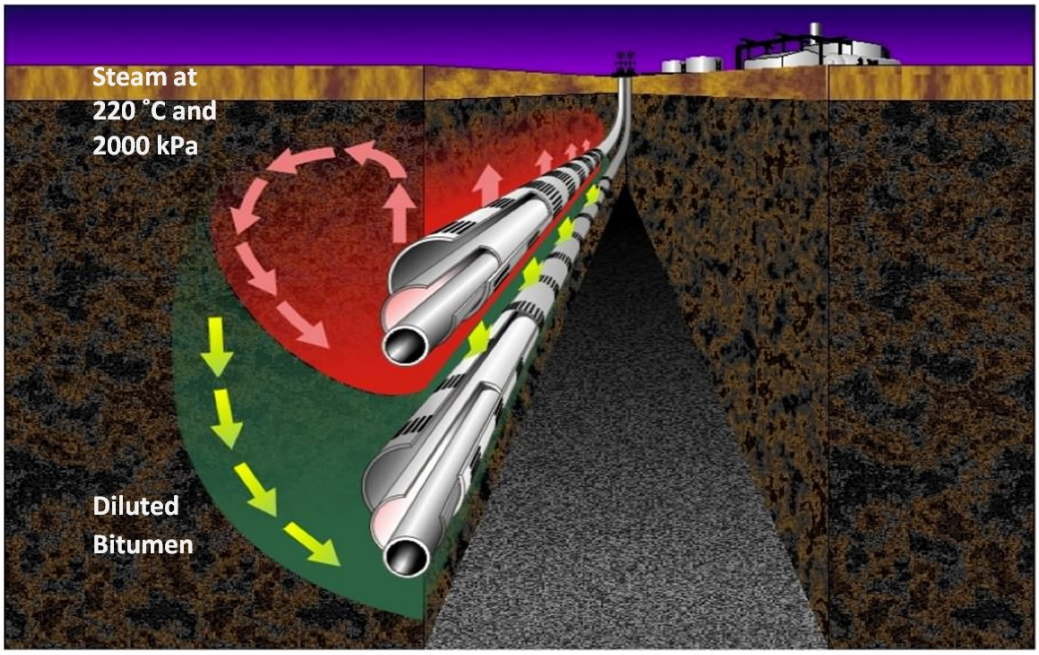

Figure 1.1: Schematic view of the principle of a typical SAGD process

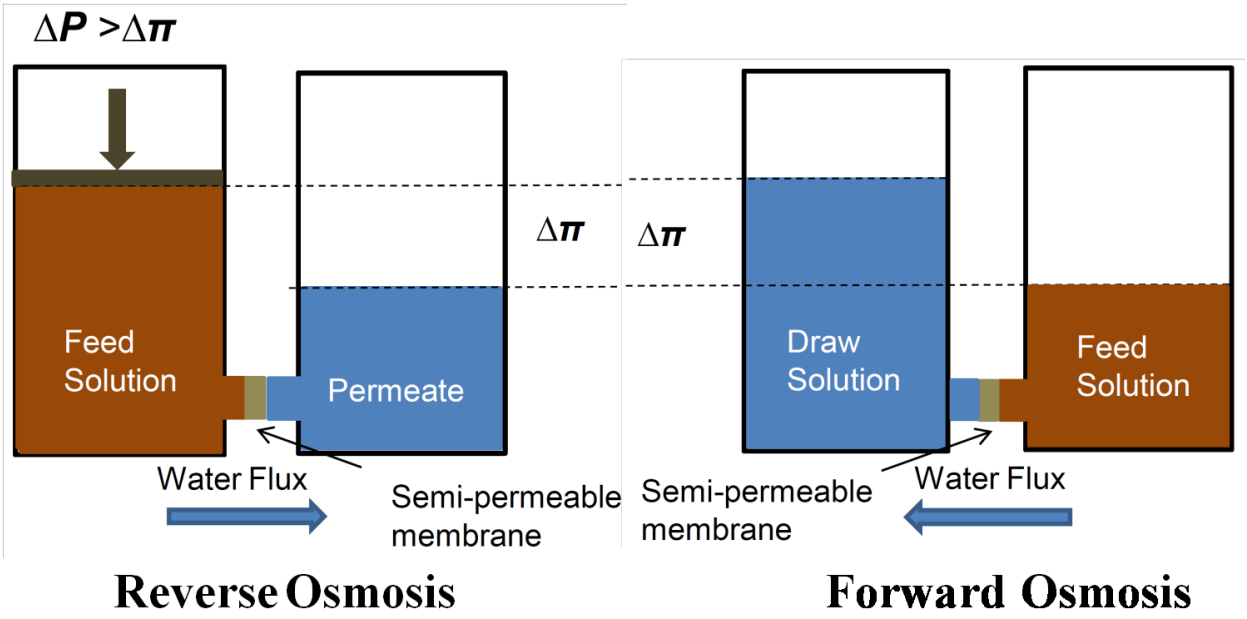

Figure 1.2: Different mechanisms of RO and FO processes. In FO, ΔP (applied hydraulic pressure) is zero and the water flows through the membrane due to the difference in osmotic pressure of the solutions. In RO, water diffuses through the membrane due to the applied hydraulic pressure (Figure adapted from [33]).

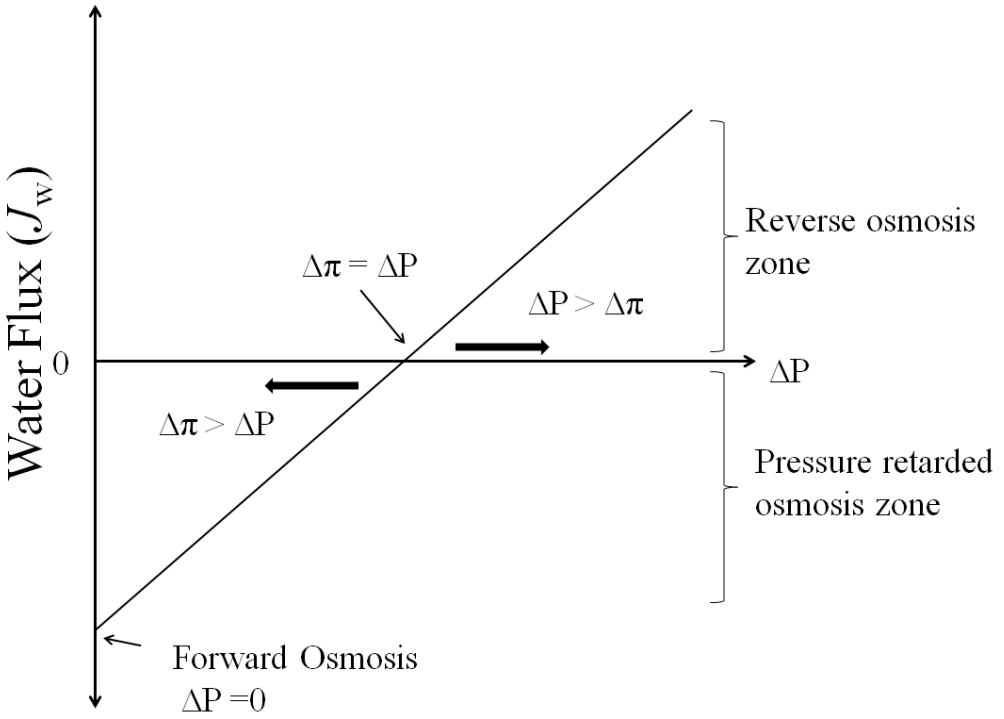

Figure 1.3: The relation of water flux and its direction for RO, PRO and FO process. FO takes place when there is no hydraulic pressure ($\Delta P = 0$). For PRO process $\Delta P < \Delta \pi$ and at $\Delta P = \Delta \pi$ there is no flux through the membrane and it is known as the flux reversal point. After this point, RO occurs when $\Delta P > \Delta \pi$ (Figure adapted from [33]).

CHAPTER 2: FORWARD OSMOSIS FOR TREATMENT OF OIL SANDS PRODUCED WATER: SYSTEMATIC STUDY OF INFLUENTIAL PARAMETERS

2.1 Introduction

Steam assisted gravity drainage (SAGD) is a thermally enhanced heavy oil recovery method which is widely practiced for bitumen extraction from oil sands in Alberta, Canada. In this process, steam is injected through a horizontal well into the bitumen-containing formation to decrease the viscosity of the bitumen and affect its extraction. An emulsion of steam condensate and heated bitumen flows down along the periphery of the steam chamber to the production well which is located below the injection well. This emulsion is then pumped to the surface where the bitumen and water are separated and the water is treated for reuse as boiler feed water [59].

Fig. 2.1 shows a conventional SAGD water treatment plant. After initial bitumen-water separation, the produced water is de-oiled by gravity skim tanks and induced static flotation (ISF) where the majority of the oil is removed from the water. Finally, the free oil content in the produced water is reduced to below 20 mg/L by passing it through walnut shell filters. The de-oiled water is then treated in a warm lime softener (WLS) for the removal of silica, followed by removal of suspended solid in after-filters. Finally, a weak-acid cation exchanger (WAC) is used to remove the residual multivalent cations like Ca^{+2} and Mg^{+2}. After the treatment process, this water is then used as feed water in once through steam generators (OTSGs).

The conventional treatment process is not designed to remove TDS and dissolved organic matter. Typical SAGD water composition after conventional treatment is summarized in Table 2.1. For this harsh quality of water, having a high level of TDS and silica, to be used as boiler feed water, OTSGs are used. OTSGs are robust and are able to handle BFW containing higher level of TDS (< 8000 ppm) and Ca/Mg/Si than conventional drum boilers [12]. To compensate for the poor water quality, the quality of steam in the OTSGs is typically limited between 75% to 80% to ensure that a sufficient volume of water is available for cooling the inner surfaces of the tubing in the radiant section and to prevent any impurities in the BFW from being deposited on the tube surface. The steam is separated from the liquid at the exit of the steam generator and is sent into the reservoir. The separated liquid is characterized by high concentration of dissolved solids and organics and is known as boiler blow down water (BBD). A portion of BBD is recycled back to the WLS while the remainder is disposed off.

Table 2.1: Specification of a typical BFW

Parameter	Units	Specification
Conductivity	mS	≈2.5
TDS	mg/L	< 2000
pH	-	9.8-10.5
DOM	mg/L	500-620
Silica	mg/L as SiO_2	< 50

The inability of the conventional water treatment method to meet BFW specifications has resulted in the fouling and failure of boiler tubes in the field [14,15]. Fouling of the boiler tubes is a major problem in the SAGD operation as it results in periodic shutdowns of the operation for cleaning and maintenance, which results in a significant loss in production of bitumen [13]. Several research efforts are being made to better understand the mechanism of fouling but still it is unclear whether the high levels of organic carbon deposited on the tubes, in addition to silica, are due to the deposition and coking of free and emulsified oil, or if they are due to temperature-related precipitation of organic matter.

In order to prevent fouling of the steam generators and to recycle as much water as possible, oil sands companies are seeking novel water treatment technologies. Membrane based separation processes have been extensively used in treating produced water due to their clear-cut advantages over conventional processes i.e. lower operating cost and energy consumption. Membrane based treatment processes have been found to be efficient in treating water with high oil content, low mean particle size and high flow rates. Numerous studies have been published on the application of microfiltration (MF) and ultrafiltration (UF) [17–22] for the treatment of oily produced water. For the separation of a broader range of contaminants like silica, dissolved organic matter and salt, tighter membrane processes like nanofiltration (NF) and reverse osmosis (RO) have been used [25,60–63]. Several studies have also been published on the use of NF and RO for treating oil sands process affected water (OSPW) associated with surface mining for bitumen extraction, and recently a study was conducted on the use of NF membrane processes for the SAGD produced water treatment [28], but to date no published studies have been found on the use of FO for the treatment of SAGD produced water. In the present study, FO was investigated for the first time on model BFW obtained from a SAGD operation to reduce the concentration of TDS and dissolved organic matter.

Forward osmosis has gained ground in the field of water treatment and desalination in the past decade [33]. Several studies have been published in the last decade showing the wide scope of application of FO in different areas of water treatment, which include desalination of seawater and brackish water [34,52], concentration of landfill leachates [53], treatment of municipal [39,64,65], industrial wastewater [55,56], and processing of food and beverages [66,67].

Cath et al. [56] used seawater as a draw solution, due to its low cost and high availability in coastal regions, to produce drinking water using water from a domestic wastewater treatment plant and impaired surface water as feed. The main motive of this study was to investigate the performance of FO in conjugation with RO. Investigation of membrane fouling tendency, rejection of inorganic compounds, nutrients and also preliminary

economic evaluation of the hybrid system were done. Great improvement was observed in terms of rejection, low membrane fouling and low cost with a dual barrier FO-RO process. Hutchings et al. [50] tested the applicability of FO for reclaiming drilling wastewater for reuse as the base fluid for hydraulic fracturing. The system operated with a 26% w/w NaCl draw solution for treating a drilling wastewater with a 5000 ppm TDS concentration. The FO system was able to recover 70% of the water from a typical wastewater pit and a significant reduction in the concentration of heavy metals and salts was found in the recovered water. Another study was made by Hickenbottom et al. [57] on FO operation for the treatment of drilling mud and fracturing wastewater. Bench scale tests were performed on waste streams using a commercial CTA membrane and a 26% w/w NaCl draw solution. It was reported that at least 80% of the O&G drilling wastewater volume was recovered. A high rejection of inorganic and organic compounds was achieved during the pilot testing. Minimal irreversible fouling was observed and the effectiveness of osmotic backwashing to remove the fouling layer was also demonstrated.

The above mentioned studies investigated the general feasibility of FO, but did not determine optimal performance parameters. The performance of the FO system depends upon various parameters like temperature, flow rate, draw solution concentration and the pH of the feed, which will affect the water flux as well as the rejection rate of the membrane. In this study, the effects of all major factors like temperature, flow rate and pH of the feed water and the concentration and flow rate of the draw solution on the FO of model BFW obtained from a SAGD operation were investigated. The undesired diffusion of organic matter toward the draw solution was also reported. Since no interaction between parameters was predicted, a fully saturated L_{16} Taguchi design was used to investigate these five parameters each at four levels. Using a Taguchi experimental design, the results of the experiments were analyzed to identify 1) the optimal process conditions in terms of water flux, 2) the role of individual parameters and 3) the response for the conditions which were not experimented. Analysis of variance (ANOVA) was used for statistical analysis of the results and also to determine the contribution of each factor towards response variation.

2.2 Materials and Methods

2.2.1 Preparation of feed

A model SAGD BFW was prepared by diluting BBD water obtained from a SAGD treatment plant located in the Athabasca oil sands region of Alberta, Canada. Hot samples were collected, shipped in sealed containers, and were kept in an inert atmosphere with a nitrogen blanket. 950 grams of BBD water was diluted five times to obtain the properties of BFW. 1 M NaOH and 1 M HCl (Sigma Aldrich) were added to the model BFW to get the required pH of the solution.

2.2.2 Membrane

A semipermeable polyamide thin film composite (TFC) membrane with embedded polyester screen support was acquired from Hydration Technology Innovation (HTI Albany, OR). Based on manufacturing data, the maximum operating temperature and workable pH range of the TFC membrane was 71˚C and 2 to 11, respectively. In the present work, the threshold operating conditions were deliberately reached to test the membrane filtration performance under the harsh conditions which would be expected during full-scale industrial application of the system.

2.2.3 Crossflow forward osmosis setup

A bench scale forward osmosis test cell system was obtained from Sterlitech Corporation to evaluate the performance of the FO membrane under varying operating conditions. The schematic view of the FO setup is shown in Fig. 2.2. The system consists of two 9-litre tanks one for the draw solution and the other for the feed solution, connected to the FO membrane element cell. The effective filtration area of the cell is 140 cm^2. Variable speed gear pumps were used to circulate the solution through the system. The flow rate, conductivity and temperature were measured using digital sensors which came integrated with the system and the reading could be conveniently taken from the control panel screen on the system. A 16 kg weighing balance (Mettler Toledo, model: MS16001L,

Switzerland) was used to measure the change in the weight of the draw tank. The temperature of the feed side was increased by circulating bath heater (Polyscience, model: MX-CA11B, USA) while the temperature of the draw solution was controlled by a re-circulating chiller (Polyscience, model: 6560M11A120C, USA).

2.2.4 Total organic carbon (TOC) analysis

Draw solution samples collected at the end of the experiment were analyzed for total organic carbon (TOC), which is the indicator of the amount of dissolved organic carbon present in the SAGD produced water. TOC was measured by using a combustion type TOC analyzer (Shimadzu, model TOC-V; detection range 3-25,000 mg/L). The TOC analyzer is sensitive to high salt concentration in the solution, so the samples were diluted 10 times before they were sent for analysis.

2.2.5 Experimental methodology

To study the effect of all the influential parameters on the water flux one at a time, 4^5 numbers of experiments would have to be carried out. Instead, the Taguchi method was used for the experimental design to study the effect of all factors with minimum number of experiments. The Taguchi method utilizes orthogonal arrays to group the parameters affecting the result and the levels at which these parameters should be varied, thus significantly reducing the number of experimental configurations. The advantage of using orthogonal arrays is that it is possible to separate out the effect of each factor at a different level. For example, the mean response ratio for temperature at 25˚C, 40˚C, 50˚C and 55˚C (as given in Table 2.5) can be calculated by taking the average of the response for the experiments 1-4, 2-8, 8-12 and 8-16, respectively. The mean response for other factors at each level can be calculated in a similar way [68].

The results obtained from the set of experiments as described in the orthogonal array are analyzed in the Taguchi method using a statistical index of performance called signal-to-noise (S/N) ratio. The S/N ratio is the function of both the mean and the standard deviation of the result. Therefore, the S/N ratio is the logarithmic (to the base 10) ratio of

the mean (result) to the deviation (noise) of the result from the desired value. Depending upon the quality characteristic to be optimized, there are three standard S/N ratios (i) bigger-is-best, (ii) smaller-is-best and (iii) nominal-is-best [69]. In our study the quality characteristic to be optimized was the water flux, so the bigger-is-best response was chosen. For the bigger-is-best response, the following relation is used to find the S/N ratio:

$$S/N = -10\log\left(\frac{1}{n}\sum_{i=1}^{n}\frac{1}{J_{w_i}^2}\right) \tag{2.1}$$

where, n is the number of all observations used for the calculation of the S/N. Whatever may be the quality characteristic, the transformations of the S/N ratio are such that it is always interpreted as the bigger-the-better [69]. After analyzing the signal-to-noise ratio, analysis of variance (ANOVA) is performed for estimating error variance and for determining the relative importance of various parameters.

Five factors, each with four levels, were chosen for the experiment as shown in Table 2.2. The experimental matrix was designed by selecting a L_{16} orthogonal array. The layout of the L_{16} array used for the experimental design is presented in Table 2.3.

Table 2.2: Controllable factors and their levels

Factor	Levels			
	1	2	3	4
Feed temperature (˚C)	25	40	50	55
Feed pH	8.5	9.5	10.5	11.5
Feed flow rate (LPM)	0.5	1.0	2.0	3.0
Draw conc. (M)	0.5	1.0	2.0	3.0
Draw flow rate (LPM)	0.5	1.0	2.0	3.0

2.2.6 Experimental procedure

Sixteen experiments were conducted as shown in Table 2.3 to evaluate the performance of the FO membrane. The initial draw (NaCl) solution and feed solution (model BFW)

volumes were 2 L and 4.75 L, respectively. The TFC membrane was operated in FO mode (i.e. the active layer was facing the feed solution). The experiments were performed under the given set of operating conditions for duration of 10 hours and the flux of the draw solution and the conductivity change of the feed and draw solution were monitored throughout the experiment. The temperature of the draw solution was maintained at 28 ±3˚C throughout all experiments. The average flux over a period of 10 hr was used for analysis in our study.

Table 2.3: Experimental design using L_{16} orthogonal array

Run No	Feed temp(˚C)	Feed pH	Feed flow rate (LPM)	Draw conc. (M)	Draw flow rate (LPM)
1	25	8.5	0.5	0.5	0.5
2	25	9.5	1.0	1.0	1.0
3	25	10.5	2.0	2.0	2.0
4	25	11.5	3.0	3.0	3.0
5	40	8.5	1.0	2.0	3.0
6	40	9.5	0.5	3.0	2.0
7	40	10.5	3.0	0.5	1.0
8	40	11.5	2.0	1.0	0.5
9	50	8.5	2.0	3.0	1.0
10	50	9.5	3.0	2.0	0.5
11	50	10.5	0.5	1.0	3.0
12	50	11.5	1.0	0.5	2.0
13	55	8.5	3.0	1.0	2.0
14	55	9.5	2.0	0.5	3.0
15	55	10.5	1.0	3.0	0.5
16	55	11.5	0.5	2.0	1.0

2.3 Result and Discussion

From our past experience and from related works in the literature, five important influential parameters which affect the water flux in FO were selected: temperature, draw concentration, flow rate of feed and draw solution and pH. Fig. 2.3(a) and (b) shows variation of flux, draw conductivity and feed conductivity with time corresponding to experiment number 2 and 9 in Table 2.3. As can be seen, the flux remains constant throughout the experiment for run 2, while it decreases with time for run 9. For run 9, this

decline in flux was partially due to exceeding the critical flux of the FO membrane. At a flux higher than a critical value, the permeation drag pushes the foulants towards the membrane surface and consequently reduces the flux. Another reason behind such a sharp flux decline is simply reduction of the driving force due to the rapid concentration of the feed as well as dilution of the draw solution. For the case where the flux is low, there is not much change in the driving force, and hence the flux decline is less.

Table 2.4 shows the experimental results for average water flux and the corresponding S/N ratio calculated using Equation 2.1. To get a better understanding of the effect of each parameter, the Taguchi method uses the plots of marginal mean and the S/N ratio, as shown in Fig. 2.4 and Fig. 2.5, respectively. These graphs are based on data given in Table 2.5. It should be noted that these graphs just show the trend effect of each factor, and it would be incorrect to use these graphs to predict values which were not experimented.

Table 2.4: Average response and S/N ratio for each run

Run No	Feed temp(˚C)	Feed pH	Feed flow rate (LPM)	Draw conc. (M)	Draw flow rate (LPM)	Avg flux (LMH)	S/N (dB)
1	25	8.5	0.5	0.5	0.5	4.4	12.8
2	25	9.5	1.0	1.0	1.0	6.7	16.5
3	25	10.5	2.0	2.0	2.0	11.5	21.2
4	25	11.5	3.0	3.0	3.0	19.3	25.7
5	40	8.5	1.0	2.0	3.0	17.0	24.7
6	40	9.5	0.5	3.0	2.0	20.4	26.2
7	40	10.5	3.0	0.5	1.0	13.1	22.3
8	40	11.5	2.0	1.0	0.5	12.9	22.2
9	50	8.5	2.0	3.0	1.0	23.0	27.3
10	50	9.5	3.0	2.0	0.5	20.1	26.1
11	50	10.5	0.5	1.0	3.0	17.6	24.9
12	50	11.5	1.0	0.5	2.0	13.1	22.3
13	55	8.5	3.0	1.0	2.0	17.8	25.0
14	55	9.5	2.0	0.5	3.0	16.0	24.1
15	55	10.5	1.0	3.0	0.5	25.1	28.0
16	55	11.5	0.5	2.0	1.0	19.8	25.9

It can be seen from Fig. 2.4 and Fig. 2.5 that draw concentration, feed and draw flow rate and temperature have positive effect on the water flux. According to Fig. 2.5(b) increasing the pH from 8.5 to 10.5 slightly increases the flux but, thereafter it has no influence. From the Taguchi design it can be concluded that the flux is highly dependent on the change in draw solution concentration and feed water temperature (Fig. 2.5(a, d)).

Table 2.5: Effect of influential parameters

Factor	Level	Response (Flux)	Response (S/N)
Temperature (˚C)	25	10.47	19.06
	40	15.87	23.82
	50	18.47	25.13
	55	19.68	25.73
pH	8.5	15.57	22.39
	9.5	15.81	23.21
	10.5	16.84	24.12
	11.5	16.27	24.03
Feed flow (LPM)	0.5	15.55	22.46
	1.0	15.50	22.86
	2.0	15.87	23.68
	3.0	17.57	24.57
Draw concentration (M)	0.5	11.65	20.38
	1.0	13.75	22.14
	2.0	17.11	24.45
	3.0	21.97	26.78
Draw flow (LPM)	0.5	15.61	22.25
	1.0	15.65	23.00
	2.0	15.72	23.67
	3.0	17.51	24.83

These results are consistent with the previous literature [70,71]. Increasing feed and draw flow rate slightly improved water flux (Fig. 2.5(c, e)). This is attributed to the decrease in the concentration polarization effect on both sides of the membrane.

2.3.1 Effect of feed temperature

The temperature of the feed solution was varied between 25˚C and 55˚C. Higher temperatures than 55˚C could not be achieved with the current setup. According to Fig. 2.4(a), an increase in temperature has a positive effect on the permeate flux. Change in the temperature of a solution influence its thermodynamic properties like viscosity and osmotic pressure as well as the diffusivity of dissolved solids. The osmotic pressure of a solution is given by:

$$\pi = icR_gT \tag{2.2}$$

where, i is the Van't Hoff factor, c is the molar concentration, R_g is the universal gas constant and T is the absolute temperature. So increasing the temperature of the feed solution will increase its osmotic pressure, which is not desirable because it decreases the net driving force in the FO process. But it was shown by Phuntsho et al. [70] that the increase of osmotic pressure with temperature was marginal and was insignificant when compared to the high osmotic pressure of the draw solution. With an increase in temperature there is also a decrease in the viscosity of the water. The pure water permeability (A) of the membrane is an inverse function of viscosity given by $A = \frac{1}{\mu R_{\mathrm{m}}}$, where μ is the viscosity of the solution and R_{m} is the intrinsic hydraulic resistance of the membrane [72]. So, the permeability of water through the membrane is increased with the decrease in viscosity, leading to an enhancement in diffusivity of water through the membrane.

2.3.2 Effect of draw solution concentration

From Fig. 2.4(c), it can be observed that the draw solution concentration has a strong influence on water flux. The standard flux equation in the FO process is given by:

$$J_{\mathrm{w}} = A(\pi_{\mathrm{D}} - \pi_{\mathrm{F}}) \tag{2.3}$$

where A is the pure water permeability, π_{D} and π_{F} are osmotic pressure of the draw and feed solutions respectively. As NaCl is well dissociated in the solution, it can be seen from Equation 2.2 that increasing the concentration of the draw solution proportionally

increases the osmotic pressure. So, higher permeate flux is observed with an increase in draw solution concentration due to the increased driving force (Equation 2.3). But in asymmetric membranes at higher concentration of draw solutions, a non-linear dependence of flux with driving force is observed, and the flux can no longer be predicted by Equation. 2.3. This is due to the phenomena of concentration polarization [71]. But the Taguchi method was not able to capture this non-linearity in the flux behavior, possibly due to the simultaneous influence of other factors on the flux.

2.3.3 Effect of flow rates

Fig. 2.4(c) and (e) show the effect of the feed flow rate and the draw flow rate on the water flux. Both the feed flow rate and the draw flow rate showed similar trends on flux behavior. As can be seen, the flux is almost unaffected by the flow rate when it is increased from 0.5 LPM to 2 LPM, but there is a small jump in the flux when the flow rate is increased to 3 LPM. Flux enhancement at higher flow rates is well studied in the literature for pressure driven processes [73,74], and a similar explanation can be applied in case of FO. For the feed side, the increase in feed flow rate will reduce the thickness of the concentration boundary layer near the membrane thereby enhancing the mass transfer coefficient. Therefore, the severity of the external concentration polarization is decreased at higher flow rates. Another factor which contributes to the enhancement of flux in real feed system is the reduced fouling tendency at higher flow rates [74,75].

The reason for moderate flux enhancement due to an increase in draw flow rate is not well established, since internal concentration polarization is the dominant phenomena on the draw solution which is not affected by the draw flow rate, as it occurs inside the porous support layer. A confirmation test (as will be shown later) showed a 28% increase in flux with a change in the draw flow rate from 1 LPM to 3 LPM when other parameters remained constant. A plausible explanation can be made based on the model developed by Suh et al. [76]. Previous researchers neglected the phenomena of external concentration polarization (ECP) on the draw side but this phenomenon can be significant at low cross-flow velocities and high flux. Neglecting reverse salt flux through the

membrane (rejection of salt by the membrane was > 95%), the water flux including the phenomena of ECP on draw side can be given by:

$$J_w = A\left[\pi_D \exp(-J_w K)\exp\left(-\frac{J_w}{k_D}\right) - \pi_F \exp\left(\frac{J_w}{k_F}\right)\right] \quad (2.4)$$

where k_D and k_F are the mass transfer coefficient of the draw and the feed side respectively. So, when the draw flow rate is increased, the ECP phenomenon is reduced, causing less difference in solution concentration in the bulk region and near the membrane. This consequently, leads to slightly higher salt concentration inside the porous support of the membrane.

But the improvement in flux cannot be explained just by the improvement in the mass transfer coefficient on draw side, another reasonable argument can be made on the basis of the dilution of the draw solution along the membrane by the inflow of permeate as given by Xu et al [75]. The phenomena of dilution of the draw solution can be severe at low cross flow velocity and high permeate flux. Excessive dilution of the draw solution may lead to a decrease in concentration potential across the membrane and thus reduce water flux through the membrane. However at higher cross flow velocity the diluted draw solution is replenished quickly, leading to an enhancement in permeate flux. It should be noted that, Xu et al. performed their study on spiral wound membranes, which have a higher membrane surface area than the flat sheet membrane used in out experiment, thus achieving a much higher dilution factor.

2.3.4 Effect of pH

The pH of the BFW obtained from the SAGD plant varies between 9.8 to 10.5, so it was very important to test the performance of the membrane at these conditions. Therefore, the pH of the feed solution was varied from 8.5 to 11.5. There was a minimal change in flux when the pH was changed from 11.5 to 8.5 (Fig. 2.5(b)). But this was contrary to what has been observed in pressure driven membrane processes. Sadrzadeh et al. [28] reported a 20% decrease in flux when the pH was changed from 10.5 to 8.5 in a nanofiltration separation process. It was observed that silica nanoparticles and organic

matter precipitated on the membrane surface at lower pH due to decreased inter-particle repulsion as well as particle-membrane repulsion, thus accelerating the formation of a cake layer. This cake layer formation choked the membrane and hence decreased the permeate flux through it. However according to the literature, the fouling layer formed in a FO process is less compact compared to that formed in a pressure driven membrane process [77]. Thus there was no noticeable change in flux when the pH is decreased from 10.5 to 8.5. Hence, it can be concluded that FO was less susceptible to fouling by the BFW as compared to the pressure driven membrane process.

2.3.5 Rejection of organics

SAGD BFW has a wide variety of organic contaminants with different chemical properties and molecular weight [78]. With the wide range of molecular weights and chemical properties the removal of organic compounds from the BFW is a big challenge. So, the efficiency of FO TFC membrane was tested for the filtration of organic compounds. The samples of draw solution were collected after each experiment and analyzed for DOM. TOC results showed that the rejection of the organics was in the range of 85% to 96%. The TOC rejection did not show any particular trend indicating that the membrane had a stable performance even at operating condition close to its threshold limits.

2.4 ANOVA

Results obtained from Taguchi can be coupled with ANOVA to determine the relative significance of each parameter on the response and also to determine whether the variation in response is due to a change of parameter level or due to experimental noise. ANOVA uses sum of squares (*SS*), degree of freedom (d.o.f), and mean square to find the associated *F* value, which is then compared to the *F* value obtained from the statistical table to check for the significance of a factor. A brief overview of the terms which we come across when using ANOVA is given below [69,79]:

The SS of a factor is given by:

$$SS_A = \sum_{i=1}^{K_A} \left(\frac{A_i^2}{n_{A_i}} \right) - \frac{T^2}{N} \tag{2.5}$$

where K_A is the number of levels of a factor A (K_A = 4 for all factors in this study), n_{A_i} is the number of all observations at level i of factor A (n_{A_i} = 8), A_i is the sum of all observations of level i of factor A, and T is the total sum of all observation. The SS of the error is computed using the following equation:

$$SS_e = SS_T - (SS_A + SS_B + ...) \tag{2.6}$$

where, SS_T is the total SS and is given by:

$$SS_T = \sum_{j=1}^{N} J_{\mathrm{w}\,j}^2 - \frac{T^2}{N} \tag{2.7}$$

Where, N is the total no of observations. The SS and SS_T are the basic calculations needed for ANOVA. From these quantities, variance can be calculated by dividing the sum of squares by the degree of freedom (v).

$$V_A = \frac{SS_A}{\nu_A} \tag{2.8}$$

where, v_A is the degrees of freedom of a factor A and is given by $v_\mathrm{A} = K_A$-1. From this, the F value can be calculated as follows:

$$F_A = \frac{V_A}{V_e} \tag{2.9}$$

where, V_e is the variance for the error term which can be obtained by calculating the error sum of squares (SS_e) and dividing it by error degrees of freedom (v_e), i.e. $V_e = \frac{SS_e}{\nu_e}$, $\nu_e = \nu_T - (\nu_A + \nu_B + ...)$ and ν_T which is total degrees of freedom equal to (N-1). Now the calculated F value is compared to the F value obtained from the statistical tables at various risks (α) using ν_A and ν_e. If the calculated value of F is greater than the extracted one, then it can be concluded that the effect of the parameter is significant.

Table 2.6: Statistical results based on experimental data

Flux -Mean					
Factor	***SS***	**dof**	**Variance**	***F***	***P*(%)**
Draw conc.	486.5	3	162.1	203.5	51.1
Temperature	401.4	3	133.8	167.9	42.1
Feed flow rate	22.8	3	7.6	9.6	2.4
Draw flow rate	20.6	3	6.8	8.6	2.16
pH	7.5	3	2.5	3.1	0.7
error	12.7	16	0.8		

Comparing the obtained value of F with the extracted value of F (F=3.24) from the table at α = 0.05, it can be concluded that the variance of all factors except pH is significant compared with the variance of error, and hence all these factors have significant effects on the response. The P value of the draw concentration and the temperature is very high as compared to feed flow rate and draw flow rate which brings us to the conclusion that draw solution concentration and temperature are the most influential factors in the FO process.

For optimizing the performance of the system, a balance should be established between water flux and rejection of dissolved organic matter. But for these experiments, the TOC results didn't follow any trend and the rejection rate varied from 85% to 96%. Hence, water flux was chosen as the sole criteria for optimization of performance. As a result, high temperature, high draw concentration, high feed and draw flow rates and the raw feed pH of 10.5 are recommended for maximizing the response.

Finally, after finding the significant factors by using the Taguchi method, the response for all combination of levels could be predicted with considerable accuracy. These predictions should be confirmed by running confirmation experiments. The results of the confirmation runs and the predicted values by Taguchi methods are presented in Table 2.7. As can be observed, the predicted results and experimental data match relatively

well. Hence, it is shown that acceptable results can be obtained from the reduced number of experiments. Some of the results predicted by Taguchi analysis are presented in Fig. 2.6.

Table 2.7: Comparison of flux results obtained from confirmation test run and by Taguchi prediction

Temp (˚C)	pH	Feed flow rate (LPM)	Draw conc. (M)	Draw flow rate (LPM)	Flux (LMH)		% error
					Taguchi prediction	Exp value	
50	9.5	1	1	1	14.7	15.9	7.5
25	9.5	1	1	3	8.6	8.6	0.1
25	9.5	3	1	1	8.8	11.1	20.7
25	11.5	1	1	1	7.2	7.1	1.4
25	9.5	1	2	1	9.0	10.0	10
40	10.5	2	2	2	16.9	17.6	4.0

2.5 Conclusion

The forward osmosis separation process was applied for the first time on SAGD BFW. The effect of all important factors (temperature, pH, draw concentration, feed and draw flow rate) on water flux were studied at the same time using a Taguchi experimental design. The TOC rejection was between 85% to 96%. The rejection of TOC didn't follow any particular trend indicating that membrane performance was not affected by high operating temperature and pH. Water flux was chosen as the sole criteria for optimization of system performance. High temperature, high draw concentration, high feed and draw flow rates and a pH of 10.5 are recommended for optimal performance of the process. ANOVA results revealed that draw solution concentration and temperature were the most influential parameters.

Less membrane fouling was observed and minimal treatment of the feed was required in the FO operation as compared to reverse osmosis and nanofiltration, which will ensure longer operations with the same membrane and reduced maintenance costs. Moderately high quality of water was achieved by the FO process at moderately high water flux,

which demonstrates the high efficiency of this process for SAGD produced water treatment. Altogether, in the near future FO can be considered as an alternative to the conventional SAGD treatment processes especially when the efforts to develop an energy efficient regeneration process for the draw solution succeed.

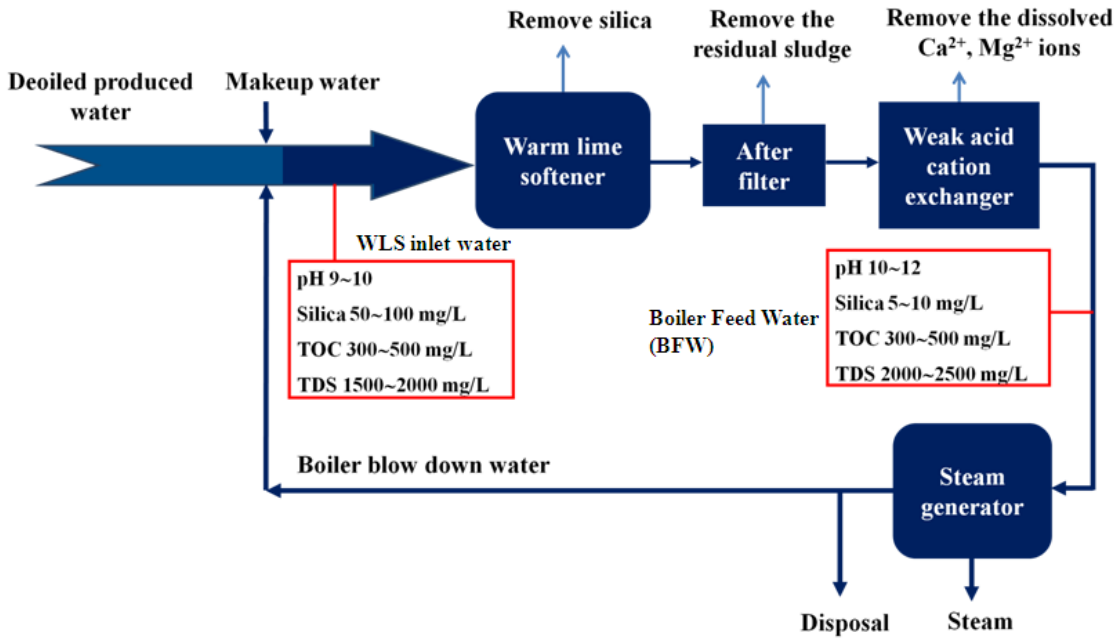

Figure 2.1: Flow diagram of a typical SAGD water treatment process (Figure adapted from [28])

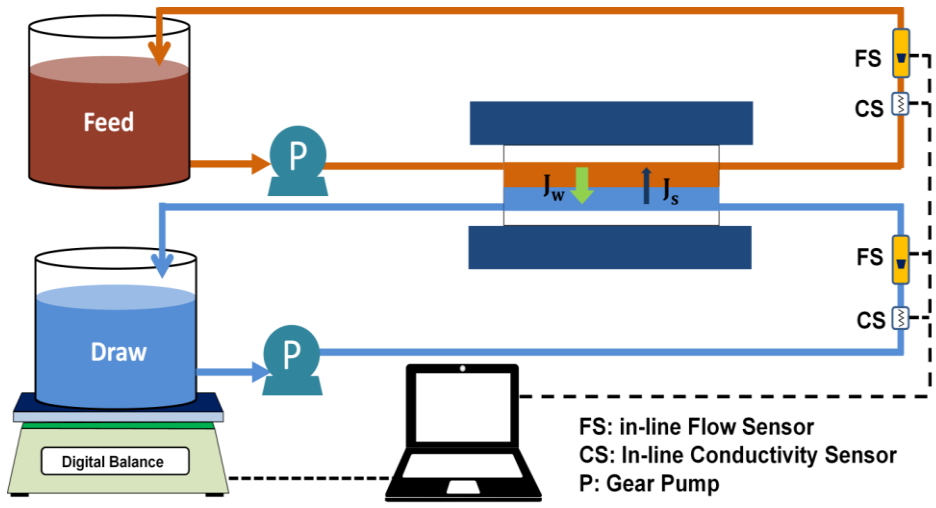

Figure 2.2: Schematic of bench scale FO setup

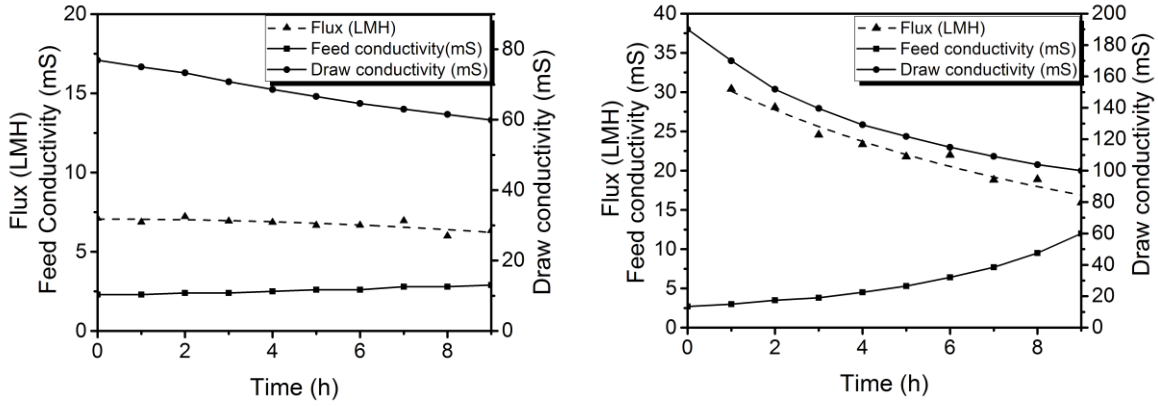

Figure 2.3: Water flux, draw conductivity and feed conductivity as a function of time for experiment no 2 and 9 corresponding to Table 2.3.

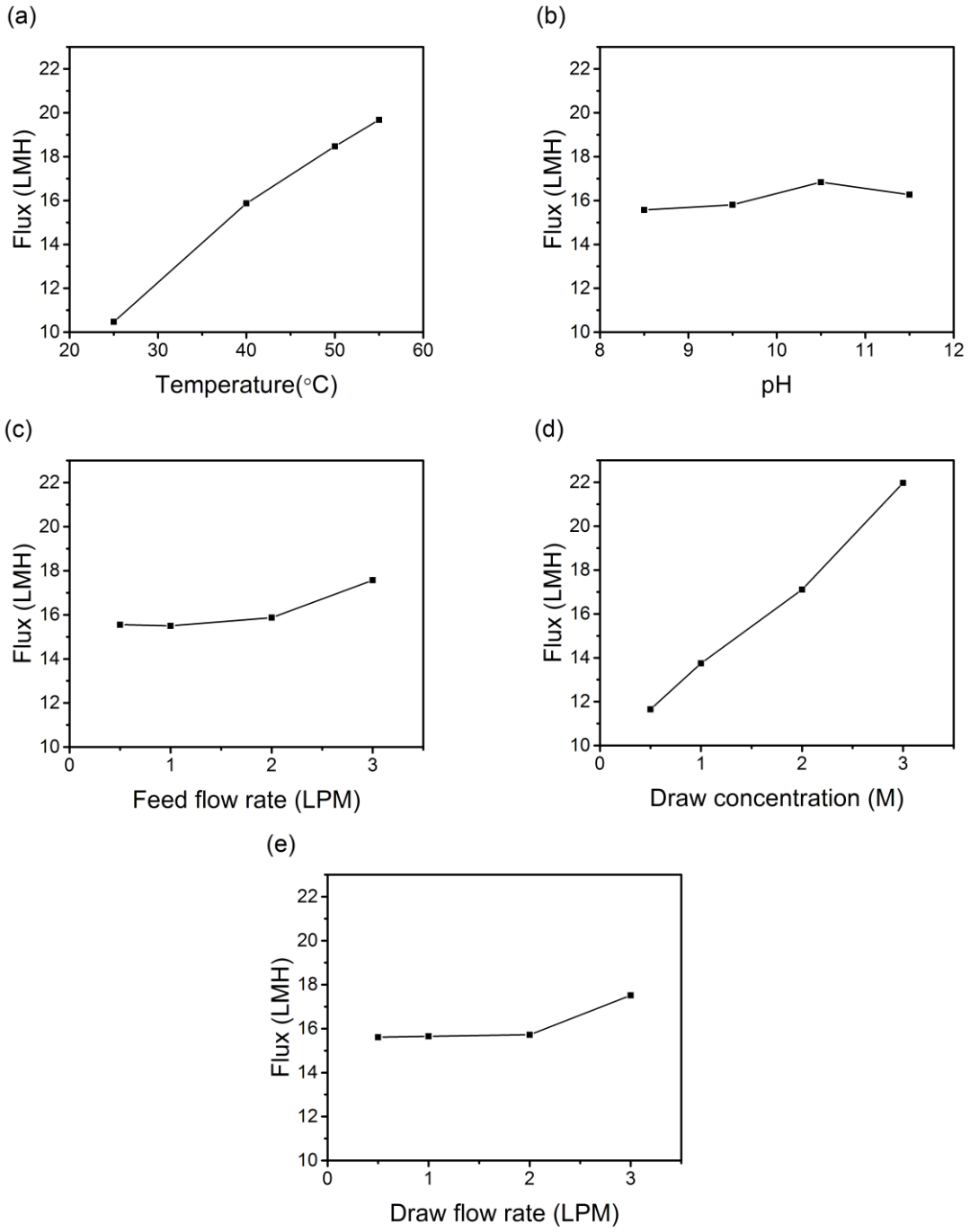

Figure 2.4: Effect of (a) temperature, (b) pH, (c) feed flow rate, (d) draw concentration and (e) draw flow rate on water flux.

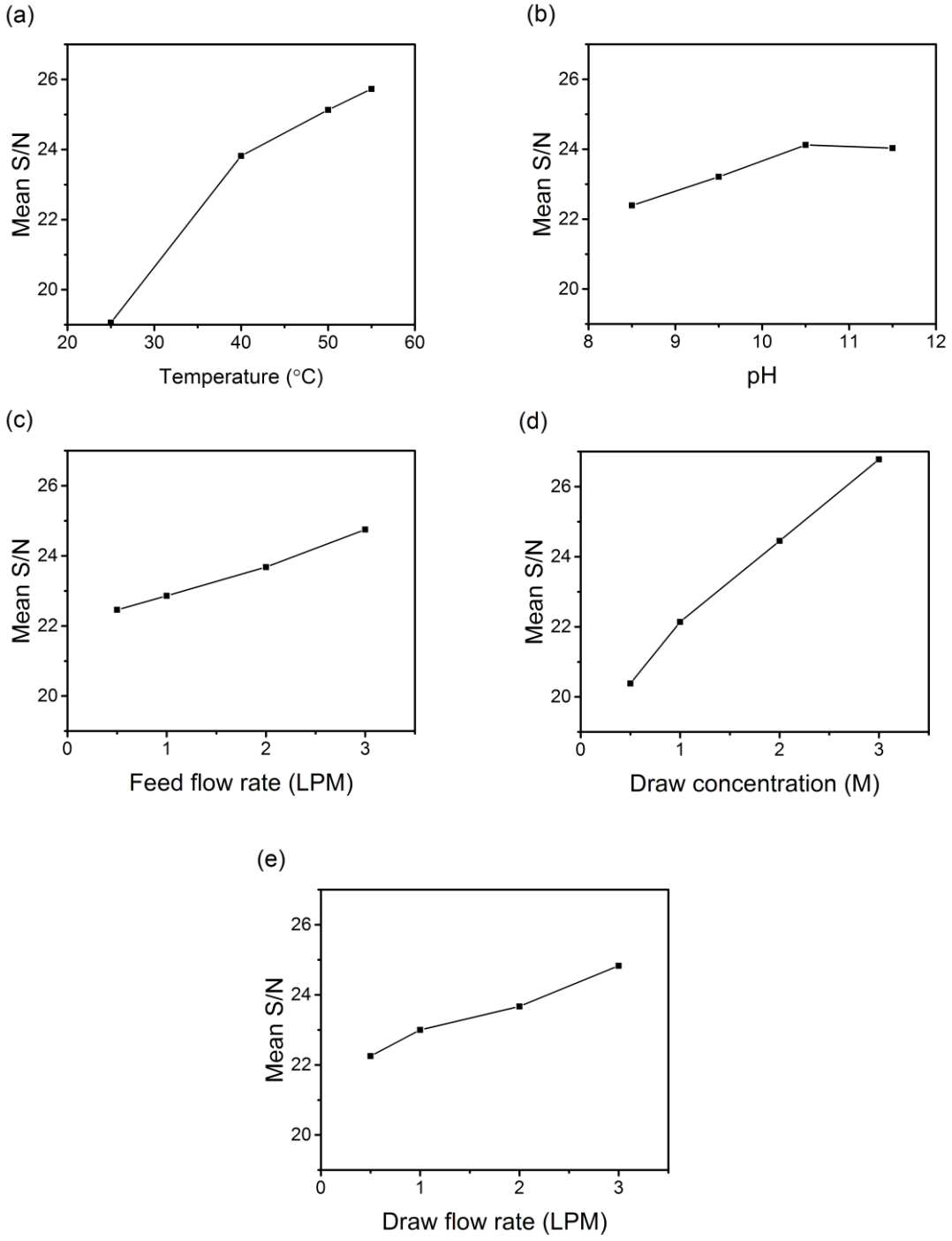

Figure 2.5: Effect of (a) temperature, (b) pH, (c) feed flow rate (d) draw concentration and (e) draw flow rate on S/N ratio.

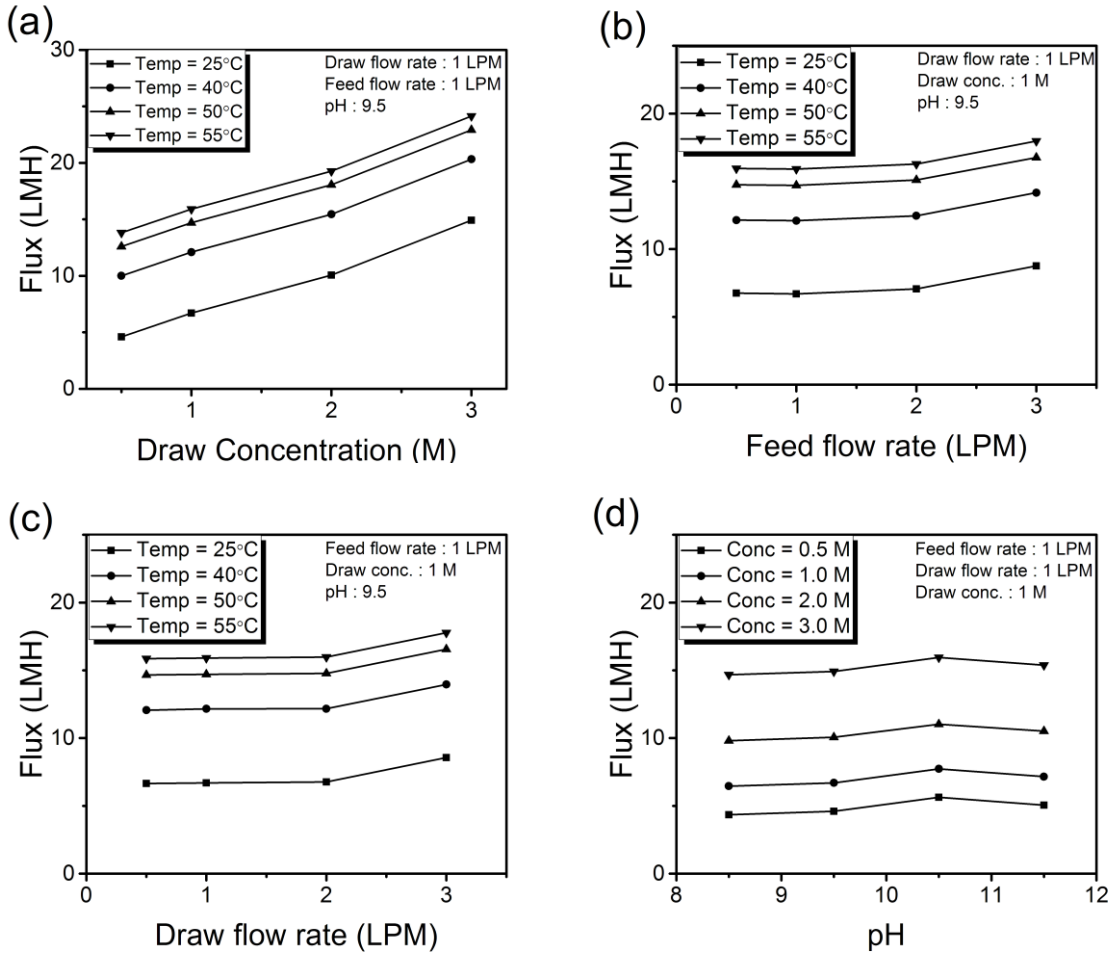

Figure 2.6: (a) Flux at different draw concentration and temperature, (b) flux at different feed flow rates and temperatures, (c) flux at different draw flow rate and temperatures and (d) flux at different pH and different draw concentration.

CHAPTER 3: MODELING OF FO PROCESS: EXPERIMENTAL INVESTIGATION OF MASS TRANSFER COEFFICIENT

3.1 Introduction

With the increasing application of membrane-based separation processes in desalination and wastewater treatment, vast efforts have been devoted to make them more energy efficient. In the hunt of more economic and efficient method, forward osmosis (FO) has been developed as an alternative to the conventional pressure-driven separation processes like reverse osmosis (RO) and nanofiltration (NF) [33,80,81]. FO is an osmotically driven membrane separation process, where water molecules are transferred from a dilute feed solution to a more concentrated draw solution through a semi-permeable membrane which selectively rejects a wide range of dissolved contaminants in the wastewater [33]. The driving force for water transport is the chemical potential difference between the draw and feed solutions, thus eliminating the use of hydraulic pressure and consequently enhances energy efficiency [35,46,57].

Besides being energy efficient, FO process is less prone to fouling as compared to pressure-driven NF and RO processes. However, FO suffers from an enhanced concentration polarization effect on the draw side where the draw solution is in contact with the porous support of the composite membrane. The severe concentration polarization reduces the real driving force for mass transfer, thereby reducing the performance of the FO process significantly [82,83]. In a typical pressure driven process, concentration polarization phenomenon occurs on one side of membrane (feed side) whereas in the FO concentration polarization happens on both sides (feed and draw). The polarization that occurs on the feed side is concentrative and is different in nature from the dilutive polarization on the draw side due to incoming permeate flux. The first type of

polarization is called external concentration polarization (ECP) and the second one that takes places inside the porous support layer is termed as internal concentration polazation (ICP). The ICP is not affected by the hydrodymanics of the flow and is more severe than the ECP which makes the theoretical study of transport phenomena in a FO process very challenging.

Early attempts to model the mass transfer through a FO membrane was conducted by Lee et al. [36]. They considered the ICP inside the porous support and developed a model to predict the performance of a pressure retarted osmosis (PRO) process. In the PRO process, which is used for energy generation from an osmotic pressure difference, the membranes are oriented in exactly opposite configuration of FO with the active layer facing the draw solution. Later, Leob et al. [84] followed the same approach and developed a model for the FO process. McCutcheon et al. [71] coupled the boundary layer film theory to capture the effect of ECP on the active layer as well as the ICP in the porous support for both FO and PRO processes. Suh et al. [76] fine-tuned this model by considering the dilutive ECP phenomenon on the draw side which was neglected by previous researchers. They suggested that the effect of diluted draw solution on the ECP must be taken into account, particularly for low cross flow velocities and high water flux. Even though the above models provide comprehensive framework of relationships for the ICP and ECP on both sides of FO membranes and are able to predict the flux satisfactorily at a certain flow rate, they are not sufficiently sensitive to the change in feed flow rate.

The change in water flux with the change in flow rate is captured by the mass transfer coefficient (k) on either side of the membrane. The mass transfer coefficient is commonly calculated using Sherwood number relations expressed in the following general form [85]:

$$\mathrm{Sh} = {}^{kd_h}\!/_{D} = c\mathrm{Re}^{a}\mathrm{Sc}^{b} \tag{3.1}$$

Where d_h is hydraulic diameter, Re is the Reynolds number and Sc is the Schmidth number, a, b and c are constants that vary for the numerous correlations of Sh number

available in literature. The most commonly used Sh number expression for a flow in a rectangular channel of a FO process are as follows: [71,76]

$$\mathrm{Sh} = 1.85\left(\mathrm{Re}\,\mathrm{Sc}\,\frac{d_\mathrm{h}}{L}\right)^{0.33} \qquad \text{(laminar flow)} \tag{3.2}$$

$$\mathrm{Sh} = 0.04\mathrm{Re}^{0.75}\mathrm{Sc}^{0.33} \qquad \text{(turbulant flow)} \tag{3.3}$$

Where Re is give by vd_h/ν, where v is the cross flow velocity in the cell and ν is the kinemetic viscosity. The Sh number relations available in the literature were either adapted from analogy between heat and mass transfer or were derived for flow in non-porous smooth [85–87]. These relations were later modified for the ultrafiltration (UF) experiments [85,86]. UF is a pressure-driven process with a different flow hydrodynamics from FO process which is driven by osmotic pressure gradient. In addition, the topology of a typical UF membrane is more rough (on a microscopic scale) and porous than a FO membrane that might affect the Sh number. Hence, the correlations of Sh number derived for UF experiments may not be valid for the FO process. Tan et al. [88] attempted to address some of these challenges by using a different correlation of Sh number developed for a fluid flow parallel to a smooth and non-porous flat surfaces. This Sh number which is theoretically developed based on the exact solutions of Navier-Stokes equation using the boundary layer concept [89] and might not be adequate in interpreting the transport phenomena in FO process.

Although extensive research has been carried out on derivation of empirical and semi-empirical Sh number correlations for pressure driven membrane processes (at various operating conditions and spacer geometries) [86,90,91], no such efforts have been made to better understand the boundary layer phenomena in a FO process. It is worth mentioning that, based on the film theory the severity of the ECP depends upon the value of mass transfer coefficent. Since the concentration profile in the boundary layer is exponential in nature a small error in the value of mass transfer coefficient may magnify the error to a large extent. Hence, in order to develop a robust model for the FO process, there is a crucial need to find an appropriate correlation of mass transfer coefficient for

each specific membrane process with a certain hydrodynamic properties of channel and membrane characteristics.

In this work an attempt has been made to get an estimate of the range of values for the mass transfer coefficient which might result in a more accurate flux prediction in a FO process. Since the support layer of a FO membrane is made from porous polysulfone (PSf) having structure and porosity as of UF membrane, the literature Sh number correlations might be valid for this side of the membrane. But for the selective layer of the membrane, which is smooth and non porous these correlations are not necessarily usable. So we propose a more practical method to get an estimate of the value of mass transfer coefficient on the active side of the membrane in a FO process by (i) RO and (ii) PRO experiments. These values of mass transfer coefficients were then used in theoretical model to predict the water flux with the change in feed flow velocity. In the final part of this study the applicability of the theoretical model with modified value of mass transfer coefficients was challenged in predicting the performance of the FO for treatment of industrial produced water obtained from steam assisted gravity drainage process (SAGD) as the feed solution.

3.2 Theory

3.2.1 Water flux in FO

Water flux in a pressure driven membrane separation process is directly proportional to the applied pressure (ΔP) and the osmotic pressure difference of the two solutions ($\Delta\pi$) [71].

$$J_w = A(\Delta P - \Delta\pi) \tag{3.4}$$

where A is the pure water permeability. In a FO process, no pressure is applied ($\Delta P = 0$) and the water flux through the membrane is just due to the difference in the osmotic pressures of the draw and feed solutions, given by:

$$J_w = A(\pi_{D,b} - \pi_{F,b}) \tag{3.5}$$

where $\pi_{D,b}$ and $\pi_{F,b}$ are the osmotic pressures of the draw and feed solutions, respectively.

3.2.2 Concentration polarization

In a FO operation, the actual flux is far less than the theoretical flux obtained from Equation 3.5 which is due to the reduction in the available driving force. On the feed side, where the solvent permeates through the membrane, the solutes are retained by the membrane increasing their concentration on the membrane surface that is referred to as concentrative ECP. The permeate entering the draw side dilutes the draw solution at the membrane surface that is referred to as diluted ECP. Fig. 3.1(a) and (b) depict concentrative ECP in a FO process and dilutive ECP occuring in a PRO process, respestively. Both these phenomena contribute to a decrease in the net osmotic driving force across the membrane and hence lowering the flux.

The ECP can be mitigated by inducing turbulence which enhances the mixing and consequently levels the concentration difference between the bulk and adjacent solution to the membrane surface. However, the concentration polarization in FO is not just limited to ECP. The structure of FO membranes is generally asymmetric, i.e. a thin active layer which governs the molecular transport rate is coated on a porous support that provides mechanical strength. In the FO mode (when active layer and support are facing the feed and draw solutions, respectively), a more severe concentration polarization takes places inside the porous support layer of the membrane, known as ICP. The enhanced dilution of the draw solution inside the porous support contributes to a huge decline in the osmotic pressure difference, thereby decreasing the flux more severely.

Internal concentration polarization

At steady state, the salt leakage J_s from the active layer (if the membrane is not perfect) originates from convective flow of solute $J_w c$ away from the active layer and diffusive flow of solute $D^{"} \frac{dc}{dx}$ toward the active layer due to concentration gradeint inside the porous support:

$$J_s = J_w c - D'' \frac{dc}{dx} \tag{3.6}$$

Where, c is the concentration of solute at any point inside support layer, D'' is the salt diffusion coefficient in the porous support and is given by:

$$D'' = \frac{D\varepsilon}{\tau} \tag{3.7}$$

Where D is the diffusivity of solute in water, ε and τ are the porosity and tortuosity of the support, respectively. Appropriate boundary conditions (as shown in Fig 3.2) are represented as:

$c = c_{D,i}$ at $x = 0$

$c = c_{D,m}$ at $x = t$

Applying these boundary conditions a relation for the concentration of solution inside the porous support near the active layer $c_{D,i}$ is derived as follows:

$$c_{D,i} = \frac{c_{D,m} + J_s / J_w}{\exp(J_w K)} - \frac{J_s}{J_w} \tag{3.8}$$

Where $c_{D,m}$ is the concentration of solution on the support layer adjacent to the bulk solution. Here $K = \tau t/(D\varepsilon)$ is defined as the solute resistivity inside the porous support. Considering a perfect membrane with 100% salt rejection, the value of J_s can be neglected and Equation 3.8 simplifies to:

$$c_{D,i} = \frac{c_{D,m}}{\exp(J_w K)} \tag{3.9}$$

The salt concentration ratio is approximately proportional to the osmotic pressure ratio of the solution, that gives:

$$\pi_{D,i} = \frac{\pi_{D,m}}{\exp(J_w K)} \tag{3.10}$$

The actual flux is generated by the concentration difference across the active layer of the membrane and is given by:

$$J_w = A(\pi_{D,i} - \pi_{F,m}) \tag{3.11}$$

Substituting Equation 3.10 in Equation 3.11, the following equation is obtained for the actual flux through the membrane:

$$J_w = A[\pi_{D,m} \exp(-J_w K) - \pi_{F,m}] \tag{3.12}$$

External concentration polarization

The concentrative ECP occuring on the feed side of the membrane can be captured by using the same differential equation and applying appropriate boundary conditions between the membrane surface and bulk solution on the feed side.

$c = c_{F,b}$ at $x = 0$

$c = c_{F,m}$ at $x = \delta_F$

Where $c_{F,m}$ and $c_{F,b}$ are concentration of solution on the membrane surface and in the bulk feed solution, respectively. δ_F is the thickness of concentration boundary layer on the active layer of the membrane. Solving the differential equation and applying the above boundary conditions the following relation is derived for the electrolyte concentration on the membrane surface:

$$c_{F,m} = \left(c_{F,b} + \frac{J_s}{J_w} \right) \exp\left(\frac{J_w \delta_F}{D} \right) - \frac{J_s}{J_w} \tag{3.13}$$

Again for a high solute rejecting membrane $J_s \approx 0$, hence

$$c_{F,m} = c_{F,b} \exp\left(\frac{J_w \delta_F}{D} \right) \tag{3.14}$$

D/δ_F in this equation is mass transfer coefficient on the feed side of the membrane (k_F). By replacing the concentrations in Equation 3.14 with the corresponding osmotic pressures and subsituting this equation in Equation 3.12, the following equation for flux is obtained:

$$J_w = A\left[\pi_{D,m} \exp(-J_w K) - \pi_{F,b} \exp\left(\frac{J_w}{k_F} \right) \right] \tag{3.15}$$

The effect of ICP in the support layer and ECP on the feed side are accounted in Equation 3.15. By considering the effect of dilutive ECP on the draw side, a concentration

boundary layer forms on the support layer of the membrane and $\pi_{D,m}$ will not be equal to $\pi_{D,b}$.

Using appropriate boundary conditions:

$c = c_{D,m}$ at $x = 0$

$c = c_{D,b}$ at $x = \delta_D$

The following equation is derived for the concentration of solution on the support layer ($c_{D,m}$).

$$c_{D,m} = \left(c_{D,b} + \frac{J_s}{J_w} \right) \exp\left(- \frac{J_w \delta_D}{D} \right) - \frac{J_s}{J_w} \tag{3.16}$$

where $c_{D,b}$ is the bulk draw solution concentration and δ_D is the thickness of concentration boundary layer on the porous support. Applying similar assumption of $J_s \approx 0$ and inserting the mass transfer coefficient on the draw side of the membrane as $k_D = \frac{D}{\delta_D}$ we get:

$$c_{D,m} = c_{D,b} \exp\left(- \frac{J_w}{k_D} \right) \tag{3.17}$$

Finally, the modified flux equation by incorporating the ICP in the support layer and ECP on both sides of the membrane is acquired as follows:

$$J_w = A\left[\pi_{D,b} \exp(-J_w K) \exp\left(- \frac{J_w}{k_D} \right) - \pi_{F,b} \exp\left(\frac{J_w}{k_F} \right) \right] \tag{3.18}$$

Similar analogy can be applied when the process is operated in the PRO mode. In this mode, the feed and draw solutions face the support and active layers, respectively. Hence, the ECP occurs on the draw side and is dilutive in nature, i.e. the draw solution becomes diluted near the membrane surface by the incoming permeate that leads to a decrease in osmotic driving force. The dilutive ECP phenomenon provides the following relation for

the ratio of draw solution concentration on the membrane surface ($c_{D,m}$) and in the bulk ($c_{D,b}$):

$$\frac{c_{D,m}}{c_{D,b}} = \exp\left(-\frac{J_w}{k}\right) \tag{3.19}$$

where k is the mass transfer coefficient on the draw side of the membrane.

On the feed side of the membrane the ICP occurs that increases the concentration of salt inside the porous support and makes it concentrative in nature, thus decreasing the driving force. The modulus for concentrative ICP can be given by the following relation:

$$\frac{c_{F,i}}{c_{F,b}} = \exp(J_w K) \tag{3.20}$$

Where $c_{F,i}$ and $c_{F,b}$ are the concentrations of the feed solution inside the porous support close to the active layer and in the bulk soltion, respectively. By incorporating the dilutive ECP and concentrative ICP phenomena in the PRO process, an analytical model, analogous to FO, is obtained as follows:

$$J_w = A\left[\pi_{D,b}\exp\left(-\frac{J_w}{k}\right) - \pi_{F,b}\exp(J_w K)\right] \tag{3.21}$$

3.3 Materials and Methods

3.3.1 Feed and draw solutions

NaCl solutions in deionized (DI) water were used draw and feed solutions. The concentration of draw solution varied from 0.25 M to 2 M, whereas the feed concentrations were adjusted in the range of 0 M to 1 M. Solution properties like viscosity, density, diffusion coefficient and osmotic pressure were taken from literature [88]. Real produced water was obtained from an SAGD operation plant located in an oil sands region of Alberta, Canada [92] and was used as feed water solution at the final stage of this study.

3.3.2 Membrane

The membranes used in this study were polyamide (PA) thin film composite (TFC) membranes provided by Hydration Technology Innovation (HTI Albany, OR). These membranes consist of a thin PA layer coated on a PSf support all embedded on a polyester fabric. The HTI composite membranes have been recently introduced and since all previous studies were based on the HTI cellulose acetate (CA) membranes, very little information is available in literature about FO using these membranes.

3.3.3 Experimental setup

The FO experiments were conducted by a bench scale cross-flow filtration setup. The schematic diagram of the setup is shown in Fig. 2.2. The membrane cell has channels on both sides of the membrane for the flow of feed and draw solutions. The length, width and depth of the channels are 145 mm, 96 mm, and 2 mm, respectively. The effective filtration area of the membrane is 140 cm^2. Feed and permeate spacers were used on both draw and feed channels in the cell to provide mechanical support to the membrane. The flow rates in the experiments were controlled from 0.5 LPM to 3 LPM by using variable speed gear pumps (Micropump, model: 070/170/172). The temperature of the experiment was maintained at 23±1˚C. The water flux through the membrane was calculated by recording the change in the weight of the draw solution with time using a weighing scale (Mettler Toledo, model: MS16001L). During the experiment the conductivity and temperature of both feed and draw solutions were monitored through the control panel.

3.3.4 Measuring real produced water osmotic pressure

Osmotic pressure of the produced water was measured using a μOSMETTE micro-osmometer (Model: 5004 Automatic Osmometer, Precision system Inc., USA). The instrument estimates the osmotic pressure by measuring the depression in the freezing point of the solution. The osmotic pressure of three different feed samples was measured and a linear relationship was obtained between the osmotic pressure and the feed

concentration. Using this calibration plot the osmotic pressure of produced water solutions could be obtained at different concentrations.

3.3.5 Experimental Methodology

Experimental runs for both FO and PRO modes were conducted following a similar methodology. The membranes were kept in the DI water for about 24 hours before experiments. After mounting the membranes in the module, the experiments were started and the flow rates of the feed and the draw solutions were adjusted at desired values. The system was allowed to stabilize and then the change in weight of the draw solution was recorded over time. For changing the concentration of the draw solution during operation, a certain amount of concentrated solution of NaCl (5M) was gradually added to the solution. The conductivity of the draw solution was monitored online and addition of NaCl solution stopped when the conductivity of the draw solution reached to the desired concentration of the solution. Similar procedure was followed to increase the concentration of the feed solution.

3.3.6 Estimation of mass transfer coefficient

The value of mass transfer coefficient depends on the hydrodynamics of the flow, applied driving force, water flux through the membrane, characteristics of the membrane (roughness and porosity) and the type of solute [86]. In this section we provide two different methdologies to find the mass transfer coefficient: (i) pressure-driven method using RO and (ii) osmotic pressure-driven method using PRO.

Mass transfer coefficient in RO

The film theory is generally applied to capture the effect of the ECP on a membrane surface. Using this theory, the concentration profile near the membrane surface is obtained as a function of permeation flux and mass transfer coefficient:

$$J_w = k\ln\left(\frac{c_m}{c_b}\right) \tag{3.22}$$

where c_m and c_b are the concentration at the membrane surface and in the bulk, respectively. By estimating the concentration at the membrane surface, the value of mass transfer coefficient is calculated using Equation 3.22. The concentration at the membrane surface can be calculated from the osmotic pressure difference across the membrane. By measuring the water flux and salt rejection in a RO experiment and coupling these with the pure water flux, an estimate of the osmotic pressure difference across the membrane can be made, and consequently the mass transfer coefficient is calculated by the following equation:

$$k = \frac{1}{J_w}\ln\left(\frac{\Delta\pi}{2R_g T c_b R_j}\right) \tag{3.23}$$

where R_j is the salt rejection by the membrane, R_g is the universal gas constant and T is absolute temperature. The detailed procedure to derive Equation 3.23 is described elsewhere [93].

Mass transfer coefficient in the PRO mode

Using DI water as the feed solution in the PRO mode, the water flux through the membrane can be calculated by a reduced form of Equation 3.21 as follows:

$$J_w = A\left[\pi_{D,b}\exp\left(-\frac{J_w}{k}\right)\right] \tag{3.24}$$

The mass transfer coefficient can be calculated by re-arranging this equation.

3.4 Results and Discussion

3.4.1 Pure water permeability (*A*)

The pure water permeability of the membrane was acquired using a RO setup with DI water as feed solution at 23˚C. The water flux was plotted at different pressure as shown

in Fig 3.3 and the pure water permeability (A) was found to be 2.47 LMH/atm (or 6.86×10^{-7} m/(s atm).

3.4.2 Mass transfer coefficient

Fig. 3.4 shows the values of the mass transfer coefficent obtained from the RO experiments at different feed flow rates and 1600 ppm NaCl solution as feed. Although these results are obtained from a RO process, they could also be valid for a FO process as in both processes the active layer faces the feed and the pressures in RO process were set to levels which resulted in comparable fluxes to that in FO process.

The average value of mass transfer coefficient obtained from PRO experiments (averaged for different concentrations of draw solution and DI water as feed) are also presented in Fig. 3.4. As can be observed, mass transfer coefficients obtained by both experiments have the same order of magnitude of 10^{-6}. As expected, different orientation of membranes in these processes led to dissimilar coefficients which can be attributed to generation of different flow pattern on the membrane surface. However, at lower flow rates the values obtained from the RO and PRO experiments match satisfactorily well.

The values of mass transfer coefficients obtained by PRO experiment at various feed flow rates are compared with the theoretical ones (calculated by Equation 3.2) in Table 3.1. As can be seen theoretical mass transfer coefficients are one order of magnitude larger than experimental ones. Using these two mass transfer coefficients, the permeation fluxes are calculated and the results are presented in Table 3.1. Applying larger theoretical mass transfer coefficients was found to over-predict experimental fluxes by almost 100%, whereas experimental PRO values provided comparable results with relatively good accuracy.

Fig 3.5(a) shows the variation of flux in PRO experiments with the change in the draw solution concentration at different flow rates. The rate of water flux increment was found to decrease with the increase in the osmotic driving force and this is attributed due to the effect of dilutive ECP. Dilutive ECP tends to decrease the net osmotic driving force due

to the diluted draw solution on the membrane surface by the incoming permeate. According to Equation 3.19, the electrolyte concentration reduces from the bulk to the membrane surface with an exponential function of flux, thereby reducing the driving force for mass transfer. The plots in Fig. 3.5(a) were corrected for dilutive ECP and the experimental fluxes are plotted against the concentration at the membrane surface (effective driving force) resulting in linear plots as shown in the Fig. 3.5(b-e). The slope of these line gives the pure water permeability (A) of the membrane. The concentration at the membrane surface was calculated using two values of k, one obtained from Equation 3.2 and the other from the PRO experiments. It can be seen that for the values of k obtained by PRO, the slope exactly matches the pure water permeability of the membrane that was obtained from RO experiment while for the theoretical k value the slope is about half of the experimental RO result.

In Fig. 3.6 the values of k obtained from PRO experiments are compared with those given in the literature and it is found that they are an order of magnitude less than those obtained from Equation 2 (k_{Sh1}) given by McCutcheon et al. [71]. Taking a closer look at Fig. 3.6 it is found that the value of k changed with the change in cross-flow velocity but not with the permeation flux.

Table 3.1: Comparison of predicted flux evaluated by using theoretical mass transfer coefficient (Eqn 3.2) and experimental mass transfer coefficient (PRO mode) with experimental flux data for 1 M NaCl as draw solution and DI water as feed.

Flow rate (LPM)	Cross flow velocity (m/s)	Mass transfer coefficient (m/s) by PRO ($\times 10^{-6}$)	Mass transfer coefficient (m/s) by Eqn 3.2 ($\times 10^{-5}$)	Predicted flux (LMH) by using experimental k (PRO)	Predicted flux (LMH) by using theoretical k (Eqn 3.2)	Experiment-al flux (LMH)
0.5	0.05	2.50	1.0	17.3	39.56	17.80
1	0.1	2.60	1.3	17.75	45.2	18.15
2	0.2	2.80	1.6	18.86	49.92	19.17
3	0.3	3.00	1.9	19.5	53.95	20.01

3.4.3 Flux prediction

The current models developed are mainly focused on finding an accurate value of solute resistivity (K), and very less attention has been paid to find a proper value of mass transfer coefficient for FO [71,76,82]. There are no direct techniques to determine the value of the structural parameters of a membrane, primarily porosity and tortuosity, so its value is typically evaluated by fitting the experimental data to the transport model [94]. In this technique, the value of K directly depends upon the mass transfer coefficient. Hence, there is a crucial need for finding an accurate value of mass transfer coefficient.

Investigating the current models developed for FO, it was also observed that they are insensitive to a change in the feed flow rate, while our experimental results demonstrates that the flux changes moderately with the flow rate. In the previous sections it was shown that the mass transfer coefficients obtained in the present work are one order of magnitude less than those obtained from literature (Equation 3.2). So in the current study, we have critically compared the results obtained from the two sets of mass transfer coefficients.

To start with the modeling of the FO, the hydraulic permeabilty (A) and salt resistivity of the support layer (K) needs to be determined. The hydraulic permeability of the membrane is detemined through the RO setup as discussed earlier. Salt resistivity coefficient depends upon the structural parameters of the membrane like porosity, tortuosity and thickness and on the diffusion coefficient of salt (D). Since the structural parameter is an intrinsic property of the membrane, it is assumed to be constant for a particular membrane [71,82]. Salt diffusion coefficient is also constant at a particular temperature and is not changing significantly in the range of molarities studied here (0.5-2 M) [95,96]. Hence, the value of K at a particular temperature is constant and can be evaluated by re-arranging Equation 3.18.

Table 3.2 presents the experimental FO data that used to determine the value of K for the TFC membrane. All experiments were conducted at 23°C and the values of mass transfer

coefficients obtained from RO experiment were used for calculation of *K*. As expected, the *K* values were almost constant for different feed concentrations. The average *K* value of 6.9 was used for prediction of water flux.

Table 3.2: FO experiments for calculation of *K*. Tests were conducted at 23˚C and draw and feed flow rate was set to 2 LPM

Draw conc. (M)	**Osmotic pressure (bar)**	**Feed conc. (M)**	**Osmotic pressure (bar)**	**Flux (LMH)**	***K* (s/m)×10^5**
1.5	75.4	0.05	2.05	10.2	6.99
1.5	75.4	0.1	4.13	9.0	6.70
1.5	75.4	0.25	10.57	6.4	6.8
1.5	75.4	0.5	21.7	4.2	6.73
1.5	75.4	1.0	47.9	1.5	7.14
Average	-	-	-	-	6.9

In Fig. 3.7 the predicted values of water flux by the developed model are presented along with the experimental values as a function of the driving force (osmotic pressure of the draw solution). As can be observed there is a good agreement between the predicted flux and the experimental flux. It is well known that increasing the feed flow rate increases the water flux through the membrane by enhancing the mixing near the membrane surface, thereby reducing the effect of ECP (concentrative ECP in the case of FO). The change in the flow rate is reflected through the change in the mass transfer coefficient. Here we test the sensitivity of our developed model to feed flow rate variation. The draw solution flow rate was kept constant at 1 LPM while the feed flow rate was changed from 1 LPM to 3 LPM. A 0.05 M solution of NaCl was taken as the feed solution and the concentration of draw solution was varied from 0.25 M to 1.5 M. As expected, increasing the feed flow rate increased the water flux. The experimental results and the model predictions are compared in Table 3.3. The model predictions are obtained using two mass transfer coefficients, one from Equation 3.2 and the other one from RO tests in the present study. At lower flow rates both mass transfer coefficients yield reults that matches well with experimental data. However, using the values of *k* obtained from Equation 3.2, the fluxes

were found to be insensitive to flow rates, whereas our *k* values resulted in more reasonable predictions at higher feed flow rate as well.

Table 3.3: Compares the sensitivity of the model to predict change in flux with the change in the the values of *k* with the experimental results.

Draw conc. (M)	**Feed conc. (M)**	**Experimental Flux (LMH)**		**Theoretical Flux (LMH) (*k* from RO test Fig 3.4)**		**Theoretical Flux (LMH)**** $k = \frac{D}{d_h} 1.85 \left(\mathrm{Re}\, Sc \frac{d_h}{L} \right)^{0.33}$	
		Feed flow 1 LPM	Feed flow 3 LPM	Feed flow 1 LPM	Feed flow 3 LPM	Feed flow 1 LPM	Feed flow 3 LPM
0.25	0.05	3.9	4.5	3.8	4.2	4.1	4.1
0.5	0.05	5.6	7.7	5.8	6.4	6.1	6.1
1.0	0.05	8.7	10.1	8.2	9.0	8.5	8.5
1.5	0.05	9.9	11.6	9.6	10.6	9.9	9.9

**The value of *K* for this case was found using eqn (3.18) and with the values of mass transfer coefficient obtained from Sh number equation 3.2

3.4.4 Model prediction for a real waste water

The FO process in the present study is modeled using different concentrations of NaCl solution in DI water as feed water. A real wastewater (oil sands produced water in this study) is totally different from the NaCl solution as it has dissolved impurities like organic matter and colloidal particles which foul the membrane and subsequently diminish the performance of the membrane process. However, it is was shown that the fouling tendency of the membrane in a FO process is far less than that of pressure based membrane processes [38,77]. In addition, according to our earlier studies, the SAGD produced water with moderate total dissolved solid (TDS<2000 ppm) and dissolved organic carbon (TOC<500 ppm) demonstrates a low fouling potential [28,92]. Hence, we tested the feasibility of applying the developed model for prediction of water flux during filtration of SAGD produced water. The TDS content of the produced water was changing during operation in the range of 1500-2500 ppm. Hence, a calibration plot was first developed by measuring the osmotic pressure of the produced water at different TDS concentrations using a freezing point depression osmometer. A linear correlation was

found between the TDS concentration and the osmotic pressure. The estimation of mass transfer coefficient was made by considering the equivalent concentration of the NaCl in the produced water as its TDS. The experiments were carried out for the duration of 10 hours and the water flux and the conductivity of the draw and the feed solution were monitored over time. From the conductivity of the feed and the draw solutions the corresponding osmotic pressures were estimated and were used in the theoretical model. Fig. 3.8 shows the plots comparing the experimental and modeling results at various operating conditions. The modeling results are obtained by using the values of mass transfer coefficients obtained from RO tests. It can be seen that the model can predict the experimental results relatively well despite using an industrial feed water and applying the same solute resistivity (K) as our preliminary experiments with NaCl solutions as feed water.

3.5 Conclusion

In this study an effort was made to estimate proper mass transfer coefficients for a FO process. Previous studies were all based on using the Sherwood number correlation developed from the UF experiments to predict the flux in the FO process. It was observed that using the values of mass transfer coefficient obtained from literature Sherwood number correlations did not produce any noticeable change in the water flux with the change in the feed flow rate. Hence two different experiments (i) RO (ii) PRO were conducted to provide better estimation of mass transfer coefficient. Mass transfer coefficients obtained from both these experiments were one order of magnitude less than what was obtained from Sherwood number correlation. It was shown that after applying ECP correction to the PRO results using the current study mass transfer coefficients, the slope of the fit line exactly matched the pure water permeabilty of the membrane obtained by RO. For the FO experiments it was seen that the model predictions were in better agreement with the experimental data when our mass transfer coefficients were used. The main shortcoming of previous developed models, that is insensitivity of the model predictions to the change in feed flow rate was overcome by finding suitable mass

transfer coefficients. Later, the model was also used to predict the flux during treatment of a real produced water. The results obtained in this study suggest that the mass transfer coefficient (k) which mainly affects the ECP is as important as solute resistivity (K) which is reflected in ICP effect.

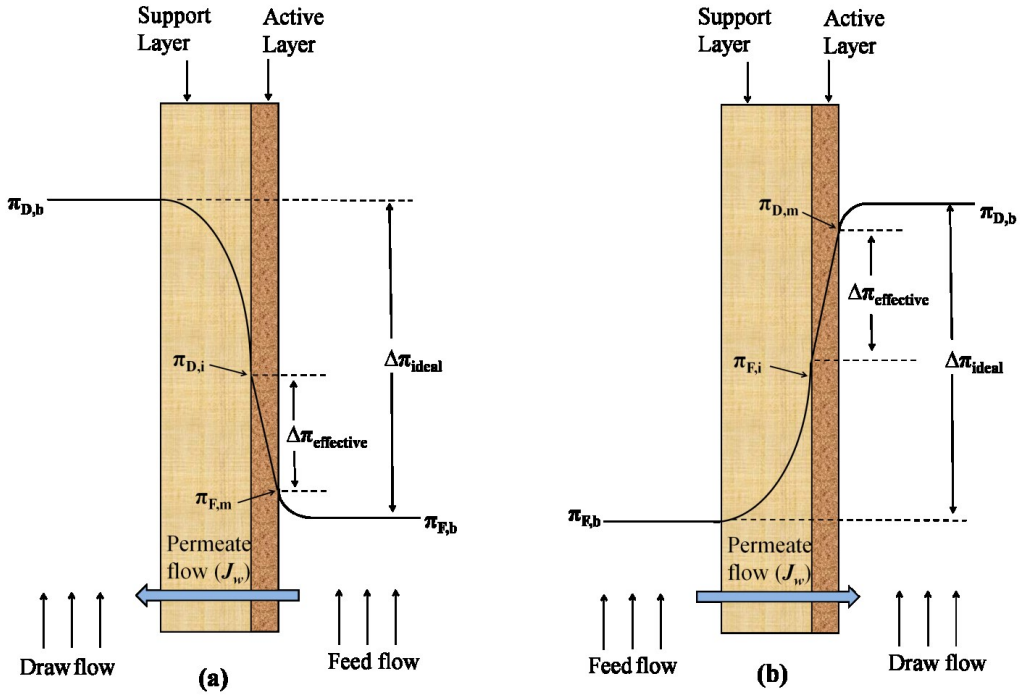

Figure 3.1: Direction of water flux and the concentration profile developed across the membrane in (a) FO mode and (b) PRO mode

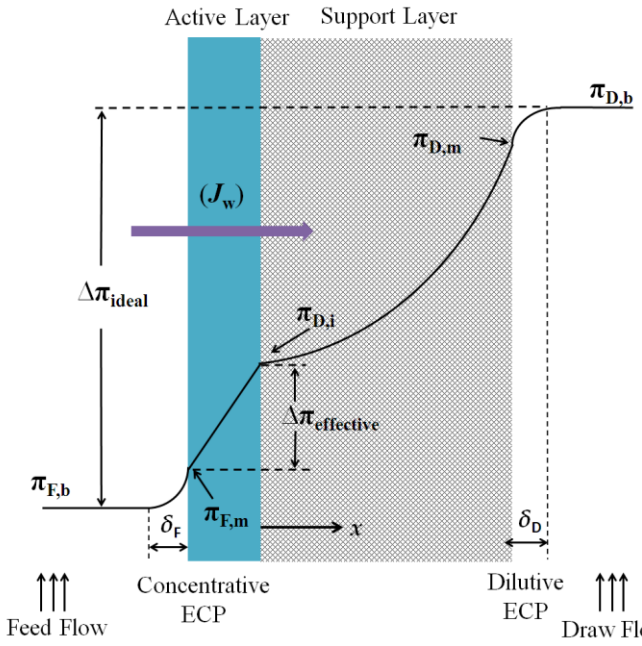

Figure 3.2: Concentration profiles (considering dilutive ECP) and the concentration boundary thickness developed on both sides of membrane during a FO process.

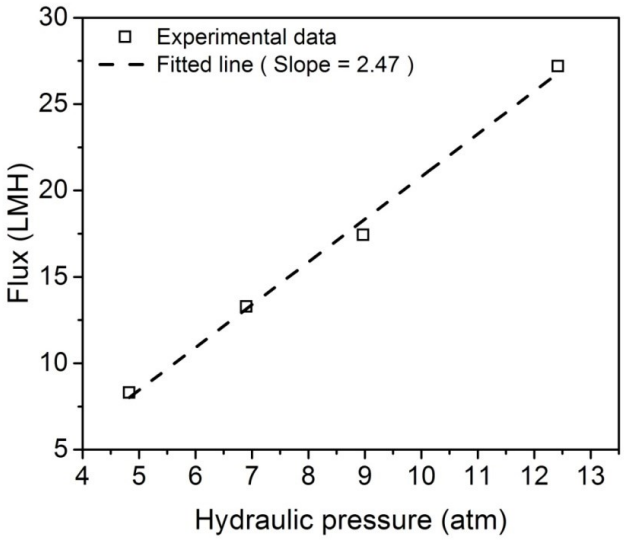

Figure 3.3: Plot of pure water flux at different hydraulic pressures in a RO setup

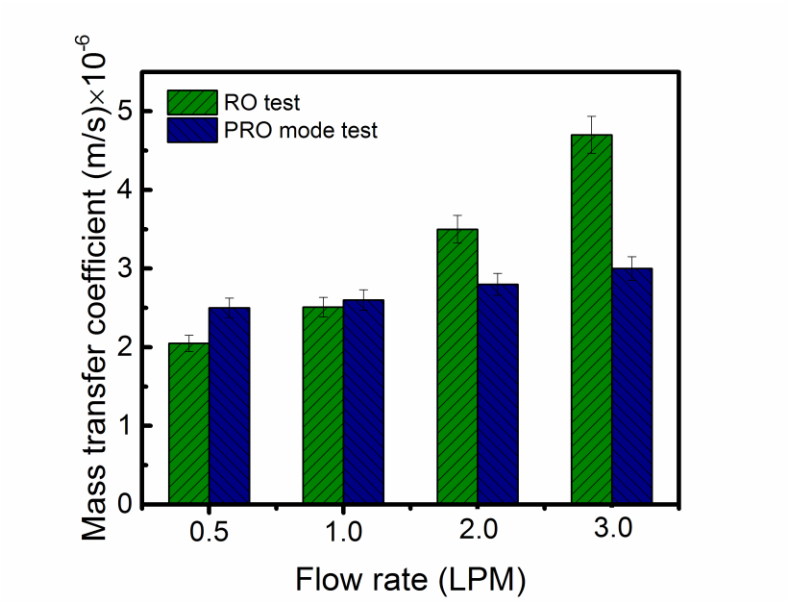

Figure 3.4: Mass transfer coefficient obtained from RO and PRO experiments. In RO experiment the NaCl concentration in feed solution and the trans-membrane pressure were adjusted at 1600 ppm and 4.0 atm respectively. In PRO experiments 0.05 M NaCl solution and the DI water were used as draw and feed solutions, respectively. The cross flow velocity varied from 0.5 LPM to 3.0 LPM for both experiments.

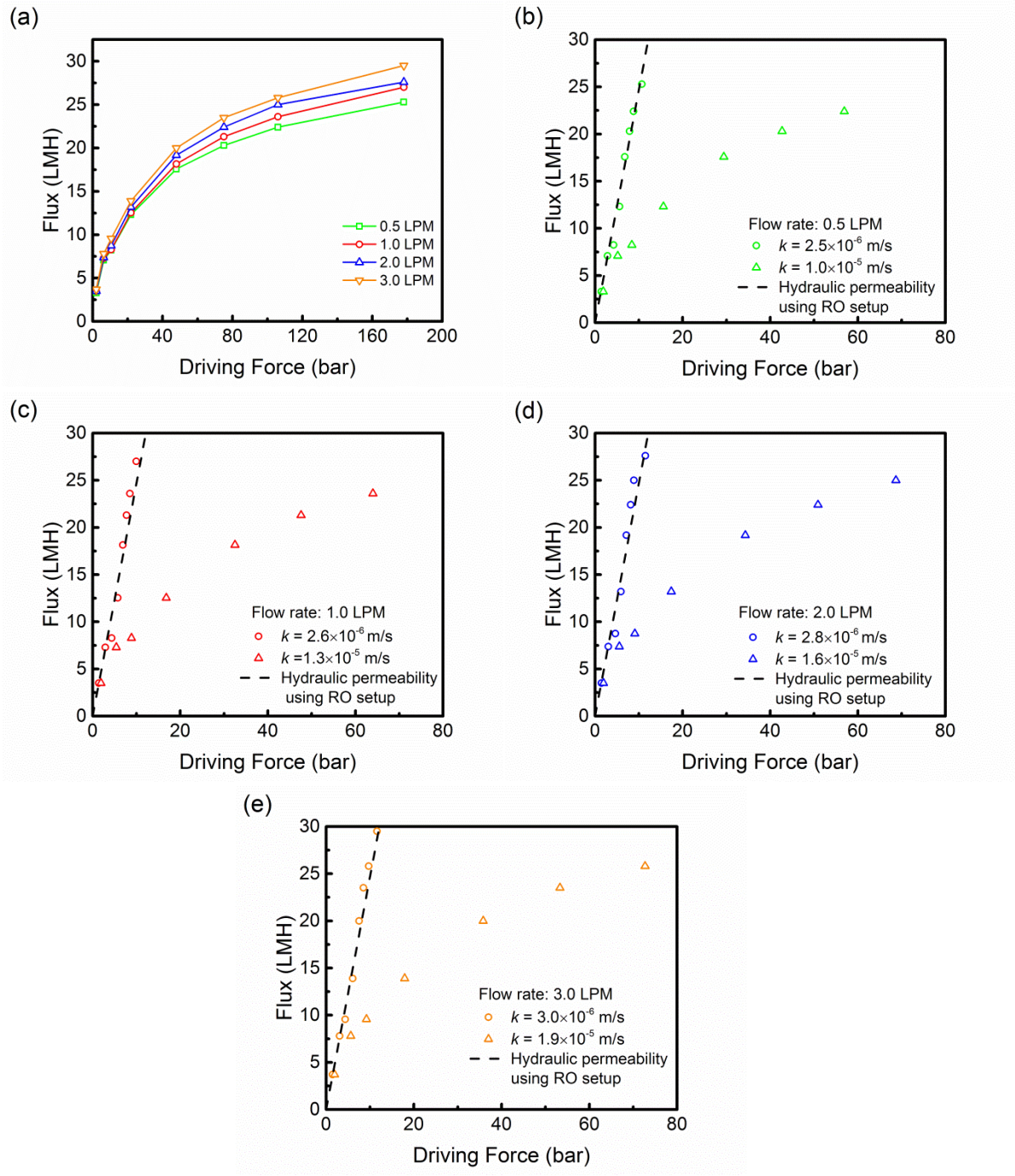

Figure 3.5: (a) Plots of flux against the osmotic pressure difference in PRO mode experiments at different flow rates (DI water was used as feed), and **(b-e)** separate plots for each flow rate after correction for dilutive ECP in PRO mode experiments for experimental (PRO) and theoretical (Equation 2) mass transfer coefficients.

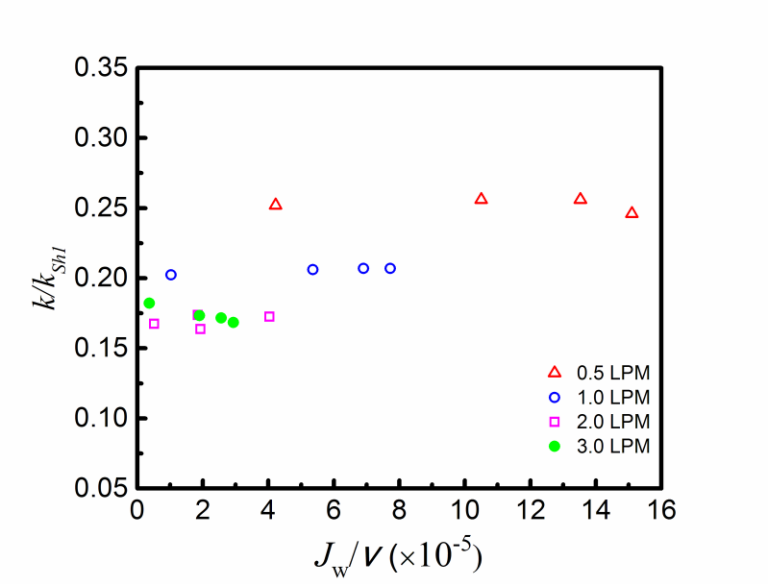

Figure 3.6: Comparison of experimental mass transfer coefficient (k) with mass transfer coefficient obtained by McCutcheon et al. (k_{Sh1}) [71] as a function of permeation flux over cross-flow velocity (J_w/v) at different feed flow rates.

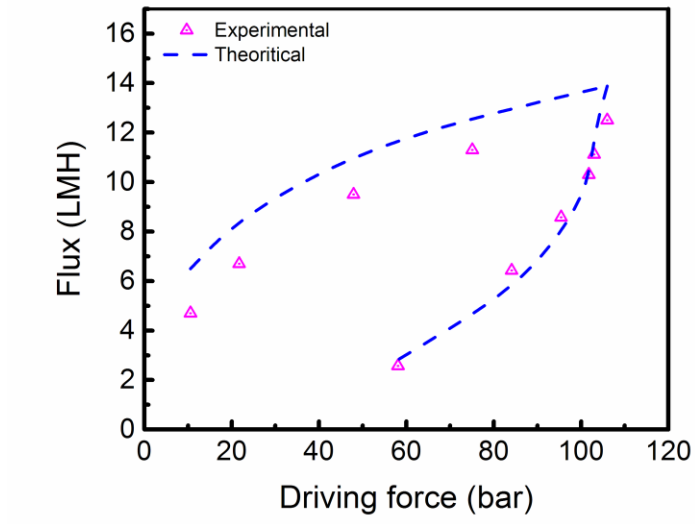

Figure 3.7: Comparison of experimental FO data and predicted fluxes by the model as a function of osmotic driving forces. The flow rate of both feed and draw solution was set to 2 LPM and the temperature was maintained constant at 23 °C.

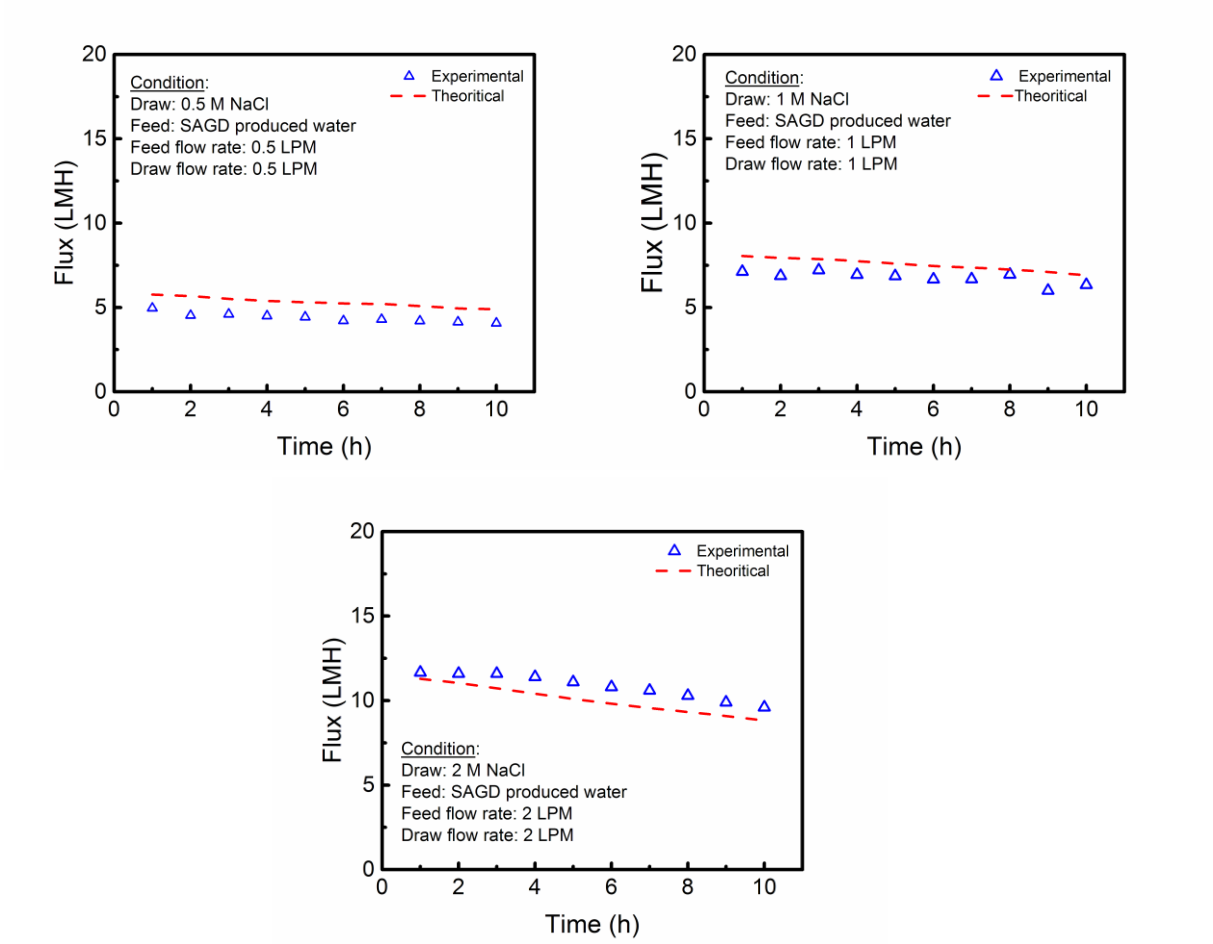

Figure 3.8: Comparing the theoretical results with the experimental data obtained from treatment of SAGD produced water treatment over time

CHAPTER 4: ULTRA THIN FILM COMPOSITE POLYAMIDE MEMBRANES FOR FORWARD OSMOSIS APPLICATION

4.1 Introduction

Forward osmosis (FO) has attracted increasing interest in the past decade as an alternative to conventional pressure-driven membrane processes for various applications including seawater desalination [4], wastewater treatment [46], food processing [33] and generation of clean energy [80,81].

The mechanism of transport in a FO membrane is based on osmosis process where water moves naturally down an osmotic pressure gradient from a low concentration solution, known as "feed", to a high concentration solution which is referred to as "draw". The utilization of semi-permeable membrane between the draw and feed provides pathways for water molecules while restricting the passage of solutes from one side of the membrane to the other side. Ideally, a FO membrane exhibit high water permeability, high solute rejection, low concentration polarization, low fouling propensity and high chemical and mechanical stability [33,97,98].

The majority of the recent advances in FO process is devoted to membrane materials development with the aim of producing high performance FO membranes [99]. Commonly used commercial FO membranes are made from asymmetric cellulose triacetate (CTA) [97,100,101] which became popular due to their hydrophilic nature and relatively low cost [80]. However, the major drawbacks of the CTA membranes are their low permselectivity and poor stability at harsh acidic and basic environment [102]. These limitation has diverted attention from single layer cellulose based membranes toward thin film composite (TFC) polyamide (PA) based membranes for FO process.

A typical TFC membrane comprises a top skin layer (~100-300 nm, mostly from PA) formed by interfacial polymerization (IP) reaction at the surface of a microporous substrate [103]. The support substrate usually consists of a polysulfone (PSF) or polyethersulfone (PES) cast over a polyester fabric, typically polyethylene terephthalate (PET), by phase inversion technique [104]. The composite structure of the TFC membranes provide beneficial flexibility in their design, as both the top active and the bottom support layers can be tailored separately to optimize the final performance [80]. Although the TFC membranes are very popular in pressure-driven separation processes like reverse osmosis (RO) and nanofiltration (NF), their application in FO is at its early stage [105].

The TFC-RO and TFC-NF membranes have typically dense active layer to provide high selectivity and a thick support layer to offer mechanical stability when external hydraulic pressure is applied. But these membranes exhibit low permeation flux when tested for the FO process, as in the absence of hydraulic pressure the dense active layer hinders the permeation flux through the membrane [33,97,100]. Additionally, the thick and the dense support layer provides a huge resistance against diffusion of draw solute to the back side of the active layer, contributing to the phenomenon of internal concentration polarization (ICP), thereby adversely affecting the water permeation of the membranes [71]. The ICP generally occurs inside the pores of the porous support layer and depends mainly upon the thickness, porosity and tortuosity of the support layer rather than the hydrodynamics of the flow [71]. Ideally, the support layer should be thin, highly porous with low tortuosity [71,82]. Hence, numerous efforts have been made on modification of the TFC membranes in terms of physico-chemical characteristics of both active and supports layers to be efficiently adapted for the FO process. Much of these efforts were dedicated to improve the support layer characteristics by the following strategies: (i) modifying the support layer morphology [97,105–109], (ii) increasing the hydrophilicity of the common support materials, i.e. PES or PSf, either by blending them with more hydrophilic materials such as sulfonated polysulfone (SPSf) [98], polyphenylsulfone (PPSU) [107], carboxylated polysulfone (CPSfs) [110] or by coating them with hydrophilic polymers

like polydopamine [100] or sodium dodecyl sulfate (SDS) [111], (iii) using alternative hydrophilic support materials like polyketone [112], sulfonated poly(ether ketone) (SPEK) [113], cellulose acetate propionate [114], cellulose acetate [115], sulfonated polyphenylenesulfone (sPPSU) [116], polyacrylonitrile (PAN) [117], (iv) incorporating nanoparticles like TiO_2 into the polymer matrix [118] and (v) using highly porous electrospun nanofibers matrix as support [119–122]

However, a few studies have investigated the modification of the active layer via tuning the synthesis reaction parameters [117,123] or incorporating nanoparticles into the active layer of the TFC membrane [124–127].

The present work demonstrates fabrication of high throughput TFC membranes for the FO process by synthesizing ultra-thin PA film over PES microporous support. The PA film is prepared via IP reaction between m-Phenylenediamine (MPD) and trimesoyl chloride (TMC) at the surface of polyethersulfone (PES) substrate. The innovative adjustment was made by reducing the temperature of the TMC-heptane solution sufficiently below room temperature. Three TFC membranes were prepared at 25°C, 1°C and -20°C of TMC-heptane solution. The surface physico-chemical and morphological characteristics of the synthesized TFC membranes were characterized using field emission scanning electron microscopy (FESEM), transmission electron microscopy (TEM), and attenuated total reflection-Fourier transform infrared (ATR-FTIR) spectroscopy, X-ray photoelectron spectroscopy (XPS), atomic force microscopy (AFM), and contact angle measurements. Additionally, the permeation performance and structural properties of the lab-made TFC membranes were evaluated by both RO and FO tests and compared with commercially available TFC-FO membrane (HTI-TFC). Finally, the separation performance of the synthesized TFC membranes was evaluated for treatment of real waste water (steam assisted gravity drainage (SAGD) produced water).

4.2 Materials and Methods

4.2.1 Chemicals and reagents

Microporous polyethersulfone (PES, 0.2 μm) membrane was provided by Sterlitech Co. (WA, USA) and used as the support in TFC membranes. m-Phenylenediamine (MPD, ≥99%), trimesoyl chloride (TMC, 98%) and camphorsulfonic acid (CSA) were obtained from Sigma-Aldrich. Heptane (≥99%), triethylamine (TEA) and sodium dodecyl sulfate (SDS) were purchased from Fisher Scientific. All materials were used as they were received from suppliers. Commercial PA thin film composite (TFC) FO membrane with embedded polyester fabric support was acquired from Hydration Technology Innovation (HTI, Albany, OR). The industrial wastewater used for measuring the membranes permeation performance and fouling characteristics was produced water provided from a SAGD water treatment plant located in the Athabasca oil sands region of Alberta, Canada. This produced water is the inlet water to steam generator, called boiler feed water (BFW) in water treatment facilities. The pH of this water, as received was 10, and was not adjusted during the filtration experiments. Table 2.1 summarizes the properties of the BFW used in the present work.

4.2.2 Synthesis of Thin Film Composite (TFC) FO membranes

The thin film composite membranes were prepared via IP reaction between MPD and TMC at the surface of the PES support. The PES substrate was first immersed in 2 wt% MPD-water solution with 2 wt% CSA, 1 wt% TEA and 0.2 wt% SDS for 10 minutes. TEA was used as an acylation catalyst to promote the polymerization reaction by removing HCl which is formed as a reaction by-product. CSA and SDS are used to enhance the wettability and absorption of MPD solution into the PES support [128]. The substrate was then removed and excess amine solution was squeezed off the surface using a rubber roller. Next, the impregnated PES sheet was brought into contact with 0.2 wt% TMC-heptane solution to allow a polymerization reaction for 30 s. The temperature of the TMC-heptane solution was adjusted to -20°C, 1°C and 25°C using isotemperature water

bath (Isotemp 3013, Fisher Scientific) and freezer (Fisher Scientific, Isotemp™ freezer). The resultant composite membranes were then thermally cured in digital oven for 5 minutes at 70°C. Finally, the residual solution from the surface was washed away using 250 ml deionized (DI) water. The synthesized TFC membranes were then kept in the DI water bath until characterization tests were performed.

4.2.3 Characterization of PA membranes

The surface morphology of TFC membranes was observed using FESEM (JEOL 6301F). The TFC membranes were sputter coated with a thin film of chromium and imaged at a magnification of 30,000X. The cross-sectional images of the TFC membranes were examined using TEM (Philips/FEI Morgagni 268, Netherlands) at acceleration voltage of 80 kV. The samples were prepared by first staining in uranyl acetate and lead citrate, then embedding in spurr's resin, and finally sectioning using ultramicrotome (Reichert-Jung Ultracut E, USA). ATR-FTIR (Thermo Nicolet Nexus 670, USA) spectroscopy was used to study the functional groups present at surface of TFC membranes. The FTIR spectra of the samples were averaged from 512 scans and were taken over the range of 600–4000 cm^{-1} at 4 cm^{-1} resolution. The elemental composition (C, O, N) of the top 5-10 nm of the PA skin layer was analyzed using an XPS (Kratos AXIS ULTRA, UK) equipped with a monochromatic Al Kα X-ray source. Survey spectra were collected at constant pass energy of 160 eV, with a scan step size of 0.4 eV, and sweep time of 100 s in the range of 0–1100 eV. High resolution spectra for carbon (C 1s) was collected with pass energy of 20 eV, step size of 0.1 eV, and sweep time of 200 s. The surface topography of the TFC membranes was studied using AFM (Bruker Dimension Icon, USA). An area of 5 μm × 5 μm of the TFC membranes was scanned three times using tapping mode at scan rate of 1.0 Hz. The AFM data was analyzed using Nanoscope analysis software V.1.40. Analysis of the samples for the presence of organic matter was done using a combustion type total organic carbon (TOC) analyzer (Shimadzu, model TOC-V; detection range 3–25,000 mg/L). The concentration of inorganic elements such as silica, Ca^{+2}, Mg^{+2} was measured

using inductively coupled plasma-optical emission spectroscopy (ICP-OES) instrument (Agilent 735 ICP-OES).

4.2.4 Performance in RO mode

The pure water permeability and salt rejection of the TFC membranes were measured using reverse osmosis (RO) setup following standard protocol as mentioned by Cath et al. [129]. The test was performed at room temperature (23°C) and at a cross flow velocity of 0.25 m/s. The pure water permeability was measured using DI water as the feed solution at various trans-membrane pressures of 5.1 atm (75 psi), 6.8 atm (100 psi) and 8.5 atm (125 psi). The flux was allowed to stabilize at each pressure and then the corresponding flux value was plotted against pressure to obtain a linear plot. The slope of the plot gave the pure water permeability of the membrane.

The apparent salt rejection (R_j) was calculated using the following equation:

$$R_j = \left(1 - \frac{c_\mathrm{p}}{c_\mathrm{F}}\right) \times 100 \tag{4.1}$$

where c_p and c_F are the concentration of salt in permeate and feed, respectively, which are obtained based on calibration curve of the solution conductivity. Sampling was carried out after 3 h filtration of 2000 mg/L NaCl under an applied pressure of 8.5 atm at 25°C.

4.2.5 Performance in FO mode

The permeation performance of the lab-made and commercial TFC membranes was evaluated using a cross-flow FO setup. The schematic view of the FO setup is shown in Fig. 2.2. The membrane cell was designed with channels on both sides of the membrane. The length, width and height of both channels are 145 mm, 96 mm, and 2 mm, respectively, providing an effective filtration area of 140 cm^2. Thin plastic mesh spacers were used on both side of the membrane to first provide mechanical support to the membrane and second induce better mixing in the channel to reduce ECP. Pure water

permeability was measured using salt water with different concentration (ranging from 0.25 M to 3 M) as draw solution and DI water as feed solution.

The water flux through the membrane was calculated by measuring the change in the weight of the draw solution (Δm_D) passed through the effective surface area (A) of the membrane over the specific time period of experiment (Δt):

$$J_{\mathrm{w}} = \frac{\Delta m_D}{\rho_D A \Delta t} \tag{4.2}$$

where ρ_D is the mass density of the draw solution.

The separation performance of the TFC membranes was also evaluated using industrial contaminated water. The test was carried out with 0.5 M NaCl salt water as the draw solution and boiler feed water (BFW) as the feed solution. All the experiments were conducted for a period of 6 hours at room temperature (21± 2°C). The volumes of initial draw and feed solutions were 2 L. and 2.5 L, respectively. Variable speed gear pumps were used to maintain the speed of both solutions at 2.5 LPM (0.22 m/s cross flow velocity). The change in weight of the draw solution and the conductivity of the feed and draw solutions were monitored throughout the experiment. After the experiment, samples of feed and draw solutions were collected and kept in dark at room temperature until they were characterized for TOC analysis.

Membrane structural parameter

The structural parameter (S) is one of the most important properties of a FO membrane which is a measure to evaluate the vulnerability of the membrane to internal concentration polarization (ICP). The structural parameter is basically a property of the support layer and depends on the membrane porosity (ε), tortuosity (τ) and thickness (t) ($S = t\tau/\varepsilon$). The structural parameter can be obtained using the following equation:

$$S = \left(\frac{D}{J_{\mathrm{w}}}\right) \ln \frac{B + A\pi_{\mathrm{D}}}{B + J_{\mathrm{w}} + A\pi_{\mathrm{F,m}}} \tag{4.3}$$

where D is the salt (NaCl) diffusion coefficient ($D = 1.33\times10^{-9}$ m/s at 20˚C [71]), π_D is the osmotic pressure of the bulk draw solution and $\pi_{F,m}$ is osmotic pressure at the surface of membrane in the feed solutions, respectively. For high salt rejecting membranes, B is typically assumed to be zero [36].

The structural parameter of the synthesized TFC membranes and the commercial TFC membrane was evaluated using the 1 M NaCl solution and DI water as draw and feed solution, respectively. The cross-flow velocity of both draw and feed flows was maintained at 0.22 m/s. Using DI water as feed and considering 100% salt rejection, Equation. (4.3) can be simplified to:

$$S = \left(\frac{D}{J_w}\right)\ln\frac{A\pi_D}{J_w} \tag{4.4}$$

4.3 Results and Discussion

4.3.1 Scanning electron microscopy

Fig. 4.1 shows the surface and cross-sectional images of the synthesized composite membranes using the PES microporous support along with the commercial TFC-FO membrane. The PES substrate has a smooth surface with micropores in the range of 50-1000 nm. According to its cross-sectional image, the support has sponge-type structure with a thickness of about 140 μm. The surface morphologies of front and back sides of the HTI TFC membrane are presented in Fig. 4.1(b) and 4.1(c), respectively. The active surface of TFC-com membrane has the typical morphology of the polyamide-based membranes which is known as “ridges and valleys” structure. This PA skin layer is formed on a woven polyester mesh embedded in polysulfone (PSf) support as illustrated in Figure Fig. 4.1(c).

Fig. 4.1(d-f) presents the surface morphologies of the lab-made TFC membranes prepared at different temperatures of the TMC-heptane solution. The noticeable

difference in these figures is the structure of the PA skin layer which is formed during the polymerization reaction. The surface of the TFC1 membrane which was prepared at 25°C has flexuous ridges and valleys similar to the active surface of TFC-Com. The TEM image of this membrane also shows the homogeneous formation of PA film at the PES surface. However, by decreasing the temperature of the organic solution, the size of the surface features noticeably scaled down to very small protuberances in the order of 100 nm. This can be observed in the FESEM images of the TFC2 and TFC3 membranes which were prepared at +1°C and -20°C, respectively.

It is worth noting that the holes of the support layer are still visible in the surface image of TFC2 and TFC3 membranes due to the fact that an ultrathin layer of PA film was formed at the surface. However, by taking a closer look at the TEM images of these membranes, it can be seen that the support holes are internally closed by the PA layer otherwise the rejection percentage would fall down drastically. The marked reduction in the thickness of the PA active layer of TFC2 and TFC3 membranes is the main reason of high permeation performance of these membranes which will be discussed in the following sections.

4.3.2 FTIR analysis

Fig. 4.2 presents the FTIR spectra of PES support, the lab-made and the commercial TFC membranes. The FTIR spectrum identifies the peaks attributed to both the substrate and the skin layer of the TFC membranes due to high depth of penetration of IR beam at the wavenumbers of 1300-1800 cm^{-1}. The peaks at 1486 and 1578 cm^{-1} belong to the ring modes of the PES support in TFC membranes while the peaks at 1488 and 1586 cm^{-1} originates from the PSf support of the TFC-Com membrane [130]. Two weak bands at 1385 and 1365 cm^{-1} are due to methyl groups that are present exclusively in the spectrum of polysulfone [131]. Furthermore, the active layer of all TFC membranes exhibited the characteristics peaks PA at 1545 cm^{-1} (Amide II, C-N stretching), 1610 cm^{-1} (aromatic ring) and 1655 cm^{-1} (Amide I, C=O stretching) [132–134].

4.3.3 XPS analysis

Fig.4.3 presents the survey and high resolution C (1s) XPS spectra for TFC3 and TFC-Com membranes along with the chemical structure of a typical PA synthesized by IP reaction. XPS analysis provides information about the elements and the chemical bonding present at the top 1-5 nm of the PA layer. The XPS survey spectra of both commercial and self-synthesized membranes show presence of only three elements including oxygen (O 1s), nitrogen (N 1s) and carbon (C 1s) at the membrane surface. The absence of sulfur peak which is the main peak of the sulfone polymers typically used as support (e.g. PES and PSf) suggests that our synthesized membrane is defect free and the PA layer is integrally skinned on the support.

Deconvolution of C (1s) high resolution XPS spectra provided valuable information about the difference in chemical bonding of PA layer between our synthesized and the commercial membrane. The C (1s) high resolution spectra for our synthesized membrane (Fig. 4.3(b)) showed presence of three peaks, (i) a major peak at 285 eV assigned to a carbon atom without adjacent electron withdrawing atoms (C−C and C−H), (ii) an intermediate peak at 286.5 eV associated with carbon in weak electron withdrawing atoms (C−N), and (iii) a minor peak at 288.5 eV related to carbons attached to strong electron withdrawing atoms (carboxylic O=C−O and amides O=C−N) [135]. There are two distinct changes in the high resolution C (1s) spectrum of commercial membrane as compared to our synthesized membrane (Fig. 4.3(a)). First the main peak skewed to the left which demonstrates presence of more hydroxyl groups (OH) on the surface. The commercial membranes used in the present work were soaked in glycerin (having three OH groups) which indicates surface modification of these membranes with polyols (sugar alcohol) to increase hydrophilicity, thereby increasing the water flux through the membranes. Second the peak related to carboxylic acid (O=C−O) is detached from amides (O=C−N) which shows less cross-link density of the commercial TFC membrane. Fig. 4.3(c) illustrates that high linearity of the PA polymer chain increases the number of carboxylic functional groups. The contact angle value of lab-made and commercial

membranes is presented in Table 4.1. According to this table, the contact angle value of lab-made membranes decreased in the order of TFC1 to TFC3 implying that the surface wettability of the TFC membrane increased when the membrane was made with lower temperature of organic solution. Additionally, the very low contact angle (24 ±1.3°) of the commercial TFC membrane can be attributed to the hydrophilic coating layer at its surface.

4.3.4 AFM Images

The surface topography of the synthesized TFC membranes along with the commercial one is illustrated in Fig. 4.4. The ridge and valley structure observed in 2D AFM images of the TFC membranes are similar to that in FESEM images as presented in Fig.4.2. The values of average (R_a) and root mean squared (R_{rms}) roughness of the TFC membranes are presented in Table 4.1. According to this table, the average roughness of all TFC membranes is comparable and is in the range of 50-55 nm. The size of the PA ridges and valleys at the surface of the lab made membranes decreases from TFC2 to TFC3. This confirms that applying lower temperatures resulted in active layer with slightly lower surface roughness

Table 4.1: Surface roughness and surface wettability of the composite membranes

Membrane	Surface Roughness (nm)		Contact Angle (°)
	R_a	R_{rms}	
TFC1	53.0±1.6	66.3±2.4	81.2±1.6
TFC2	51.2±2.3	68.0±3.8	56.9±1.1
TFC3	49.5±2.1	65.1±2.2	53.3±1.2
TFC-Com	44.32±1.8	54.7±2.3	24±1.3

4.3.5 Separation performance

Fig. 4.5 compares the FO performance of the lab-made and commercial composite membranes. The permeation performance was evaluated over a range of osmotic driving force created by increasing the salt concentration in draw solution. According to this

figure, the water permeability of all TFC membranes increased with increase in the osmotic pressure difference between the draw and feed solutions. The rate of FO flux enhancement was high at lower values of osmotic driving forces, but it declined at higher osmotic pressure difference due to the more significant ICP phenomena in the support layer.

The comparison between the FO performance of synthesized and commercial TFC membranes revealed that all the lab-made composite membranes showed higher water permeability (J_w) than the commercial membrane. The TFC3 membrane which was prepared at lowest organic solution temperature (-20 °C) showed the highest permeability of 39.5 LMH at osmotic pressure of 179 bar. This result again confirms that the synthesis of TFC membrane at lower temperature of organic solution decreased the resistance of the membrane toward water passage by formation of a thinner PA active layer.

The intrinsic separation properties of the FO composite membranes, tested in a cross-flow RO filtration cell, are presented in Table 4.2. According to this table, the TFC3 membrane exhibited the highest pure water permeability (*A*) among all other membranes. The water permeability of this membrane is two folds higher than that of the TFC-Com (5.78 LMH/atm) compared to 2.479 LMH/atm) with comparable salt rejection percentage (93.4% for TFC3 and 95% for TFC-Com). Although the values of pure water permeability of TFC2 and TFC1 membranes were lower than the TFC com, but still they performed better in FO experiments (see Fig. 4.5) which can be attributed to their significantly lower structural parameter than the commercial TFC membrane.

Since the lab-made TFC membranes were fabricated using the same support material so they processed a similar value of the structural parameter (*S* from 436-460 μm). In general, a lower value of *S* is desirable for a membrane to counter the negative impact of ICP. With a low value of structural parameter and an ultra-thin active layer, the TFC3 yielded highest water flux whereas the flux for other lab-made membranes was compromised by the increased thickness of the active layer. It must be noted that

reduction of the active layer thickness in TFC3 is accompanied with slight sacrifice in rejection percentage of the membranes (from 97.5% in TFC2 to 93.4% in TFC3).

Table 4.2: Intrinsic properties of commercial and lab-made TFC membranes

Membrane	Water permeability *A* (LMH/atm)	Salt rejection *R* (%)	Structural parameter *S* (µm)
TFC1	0.66	97.8	460
TFC2	1.8	97.5	458
TFC3	5.78	93.4	436
TFC-Com	2.48	95.0	1770

From the FESEM images of the TFC-Com FO membrane shown in Fig. 4.1(c), it is noticed that a polyester woven fabric is used as the bottom layer to provide extra mechanical support to the membrane. The use of this woven fabric may be the reason for the high structural parameter of the TFC-Com membrane. The polyester fabric adds an extra resistance against mass transfer by increasing the solute resistivity for diffusion inside the porous support. In contrast, the lab-made TFC membrane showed higher pure water permeability owing to the presence of a thinner active layer in the one hand and lower ICP due to a lower structural parameter in comparison to the commercial FO membranes on the other hand.

4.3.6 FO separation performance with SAGD water

The permeation performance of the commercial and the synthesized composite membranes during filtration of an industrial contaminated water (BFW) is shown in Fig. 4.6. According to this figure, the lab-made TFC membranes exhibited higher water flux than the commercial membrane under similar test conditions. The initial flux for TFC3 and TFC2 was around 3 and 2 times higher than the HTI membranes, respectively. Additionally, the water flux of TFC3 membrane declined rapidly as the filtration time passes. This is mainly due to the fact that the high permeation rate of water through the membrane quickly dilutes the draw solution and at the same time concentrates the feed solution which results in a significant reduction in the driving osmotic pressure. In

contrast, for the case where the permeate flux was comparatively low, there was not significant change in the driving force leading to a very slow decline in the water flux with time.

The separation performance of TFC membranes was evaluated by measuring the amount of TOC and concentration of silica and divalent ions (calcium and magnesium) in the feed solution. The samples of feed solution were collected before and after each experiment and the rejection percentage of TOC, silica and divalent ions were calculated by establishing a mass balance between the concentration of these components in the final and initial feed solution. All the membranes had a rejection percentage of greater than 99% toward the removal of organic matters, silica and divalent ions.

4.4 Conclusion

In the present work, high performance TFC membranes were developed for FO operation by adjusting the thickness of the PA selective layer created via IP reaction over a microporous support by reducing the temperature of organic solution down to -20 °C, an ultra-thin layer of PA skin layer was formed at the support surface. It was found that the synthesized TFC membranes with tailored thickness exhibit higher permeation performance compared to the unmodified and commercial TFC-FO membranes. The results obtained in this study demonstrate the significant role of the active layer properties (thickness and morphology) on performance of a FO membrane. The microporous support used in this work had a thickness of about 140 μm with structural parameter of (451±13.1 μm). For further improvement, the support layer can be modified either in terms of structure or material to provide lower structural parameter and minimize the negative impact of the ICP, thus maximize the permeation flux.

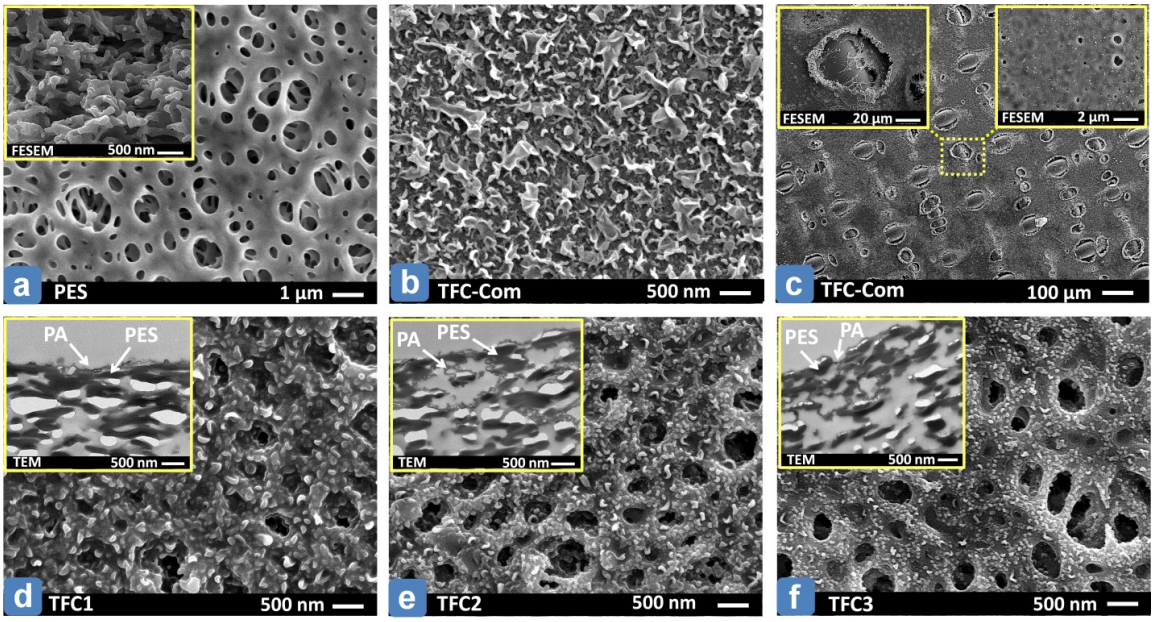

Figure 4.1: FESEM and TEM images of a) PES microporous support; b) active-side of TFC-Com; c) support-side of TFC-Com; d) TFC1 (prepared at 25 °C); e) TFC2 (prepared at 1 °C); f) TFC3 (Prepared at -20 °C)

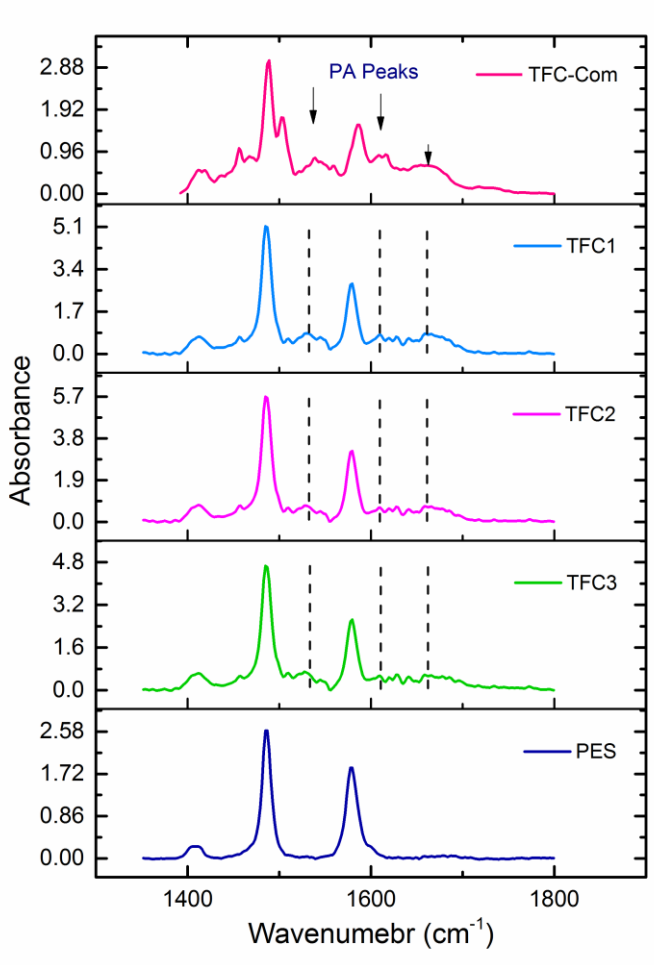

Figure 4.2: FTIR Spectra of the PES support, lab-made and commercial TFC membranes

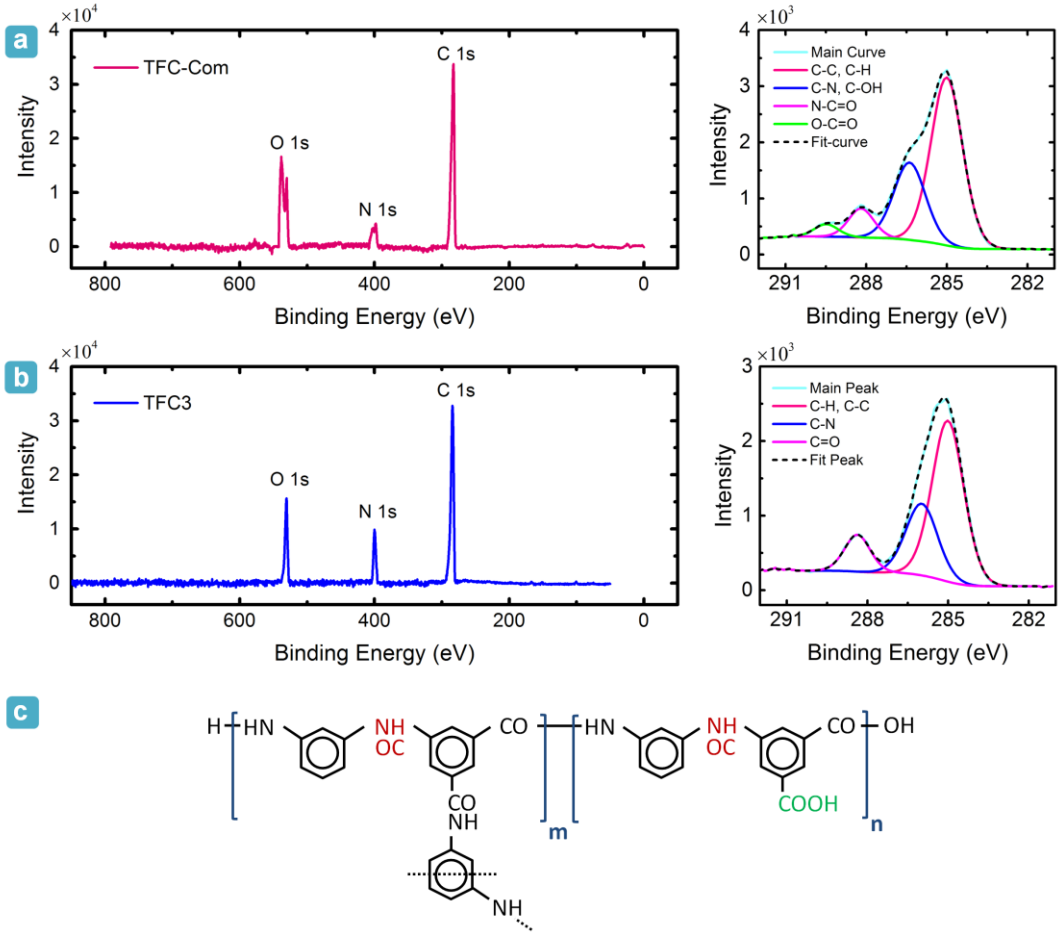

Figure 4.3: XPS survey and high resolution C 1s for a) TFC-Com and b) TFC3 membranes along with (c) chemical structure of a typical PA synthesized by IP reaction; m and n are the cross-linked and linear part, respectively.

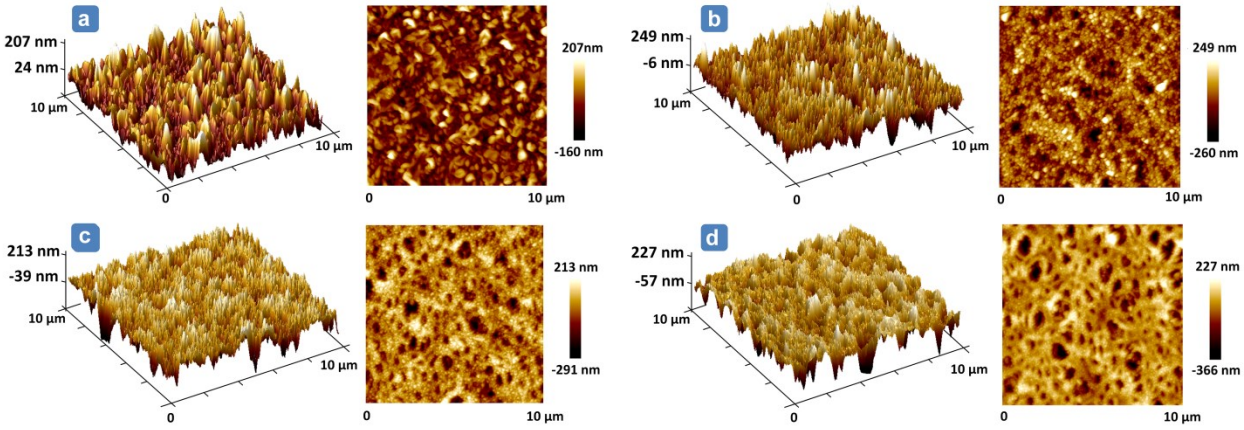

Figure 4.4: Surface topography of a) TFC-Com; b) TFC1; c) TFC2; d) TFC3 membranes

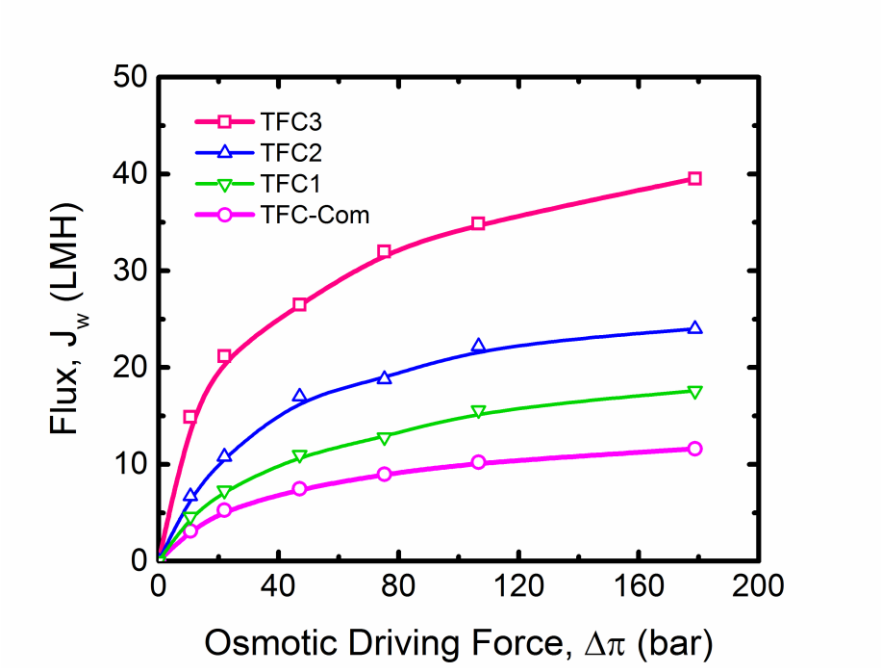

Figure 4.5: FO performance of lab-made and commercial TFC FO membranes at different osmotic pressure difference between draw and feed solutions. Test conditions: draw solution: 0.25, 0.5, 1, 1.5, 2 and 3 M NaCl solutions; Feed solution: DI water; Cross flow velocity: 0.22 m/s for feed and draw solution

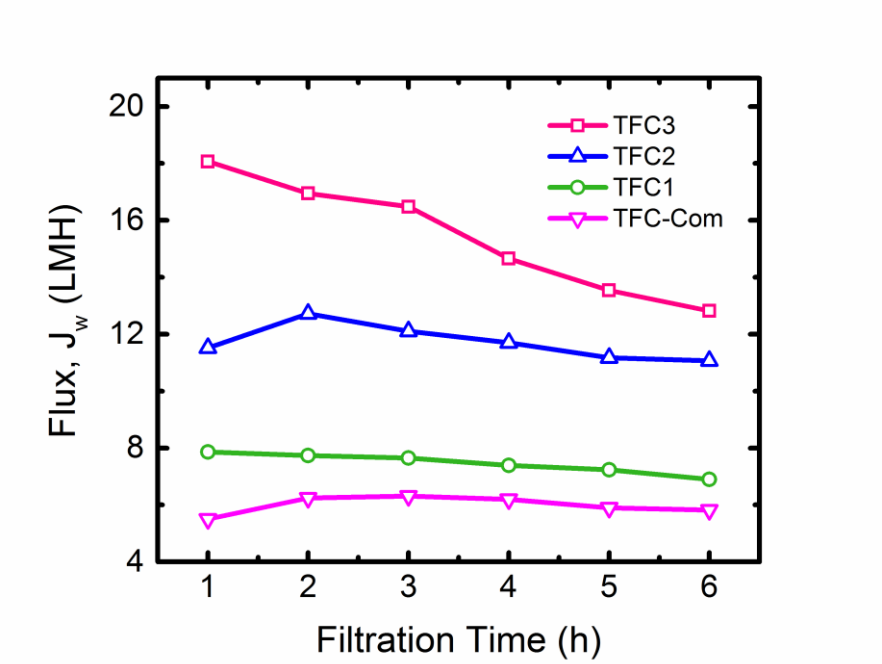

Figure 4.6: Flux performance of lab-made and commercial TFC membranes. Test conditions: Feed solution: BFW water; Draw solution: 0.5 M NaCl; Cross-flow velocity: 0.22 m/s.

CHAPTER 5: CONCLUSION AND FUTURE WORKS

5.1 Conclusion

This thesis is built on the experimental and theoretical studies conducted on the FO process for the treatment of produced water obtained from SAGD operation. The study was conducted in three stages keeping in mind the main objective, which included the feasibility test and optimization of a FO process for treatment of produced water, getting a better understanding of the FO process through modeling and fabrication of high performance TFC membranes. All these studies can be considered as a small contribution in the current application areas of the FO technology.

In the first part of the thesis, the FO process was applied for the first time for the treatment of BFW obtained from SAGD operation. The effect of important parameters such as feed water temperature, draw and feed flow rates, draw solution concentration (NaCl solution) and pH of the feed water (produced water) on the water flux as well as on the unwanted diffusion of DOM towards the draw solution were studied. As no interaction between parameters was expected, a fully saturated L_{16} Taguchi design was used to investigate the effect of these five parameters at four levels. Feed water temperature and draw solution concentrations were found to have a very high influence on the water flux. Confirmation runs revealed that increasing the temperature from 25˚C to 50˚C with other conditions remaining constant, increased the flux by more than twice for 1 M NaCl as draw solution (i.e. from 6.7 to 15.9 LMH). This was attributed to an increase in the water permeability of the membrane at elevated temperatures. Increasing the draw solution concentration also increased the water flux due to an increased driving force. Increase in the feed and draw flow rates led to a moderate increase in the water

flux by minimizing the effects of external concentration polarization. It was observed that the change in pH didn't have any significant effect on water flux. The effectiveness of a FO process to separate the organic compounds from the BFW was also tested by analyzing the samples of draw solution after each experiment. It was found that the rejection of TOC was in the range of 85% to 96%. For optimal performance of the FO process high feed water temperatures, high draw solution concentration and high feed and draw flow rates with the raw water pH (10.5) are required. This study showed that FO process is feasible for treatment SAGD produced water.

In the second part of the thesis, two experimental techniques were suggested to evaluate the value of mass transfer coefficient in a FO process: (1) PRO technique and (2) RO experiment. Previous models used the values of mass transfer coefficient obtained from Sherwood number correlations which were adapted for the UF membrane processes. However, the topology of the membrane and the mechanism of water transport in a FO process are quite different from that of a UF process. Hence the mass transfer coefficient was found experimentally from the above two methods and it was noticed that these values of mass transfer coefficient were of an order of magnitude less than the one obtained from the theoretical expressions. The ECP correction to the plot of flux versus the driving force for PRO experiments using the experimental values of mass transfer coefficient resulted in linear plots, the slope of which corresponded to the value of pure water permeability obtained from the RO tests, justifying our hypothesis that the theoretical expression Sherwood number can leads to incorrect values of mass transfer coefficient. With an increase in the mass transfer coefficient, the water flux should increase. This was observed when our experimental mass transfer coefficients were plugged in the model, while applying the literature values led to insensitivity of flux to a change in flow rates. Next this model with revised values of mass transfer coefficient was applied to predict the performance of FO when an *in-situ* oil sands produced water was used as feed solution. Generally, modeling is done for the FO processes in which the feed was a NaCl solution. But in practical situations the feed solution is a mixture of dissolved solids and organic matter which may also cause fouling, thereby reducing the flux. In the

present study the applicability of the model was tested when feed solution was actual industrial wastewater. It was found that the values predicted by the model were in good agreement with the experimental value and hence this model can be applied for the feed streams which are less harsh in nature with moderate level of TDS.

Showing the feasibility of FO to treat SAGD produced water and gaining a better understanding of the FO process, we fabricated our self-synthesized TFC membranes which could achieve higher flux than commercial membranes without compromising the rejection. Most of the studies in the literature focused on improving the support layer characteristic, i.e. the structural parameters to enhance the flux through the membrane. But much less attention has been paid to improve the active layer characteristics of a membrane. In this work, the importance of the thickness of the active layer was highlighted by making three films (named as TFC1, TFC2 and TFC3), with varying thickness of the active layer by simply controlling the temperature of the organic solution. Membranes with ultra-thin active layer was formed when the temperature of organic solution was -20˚C, having pure water permeability (A) of 5.78 LMH/atm and rejection of 93.4% (for TFC3), whereas the films formed using organic solution temperature at 25˚C possessed lowest water permeability of 0.66 LMH/atm owing to a thick active layer (TFC1). The performance of all the three membranes was then compared to the commercial TFC membrane obtained from HTI. Although the pure water permeability of the commercial membrane (2.47 LMH/atm), measured by RO test, was higher than our synthesized membranes i.e. TFC2 and TFC1 (A =1.78 and 0.66 LMH/atm for TFC2 and TFC1, respectively) however it gave lower water flux in FO experiment. This was due to a high value of structural parameter of commercial membrane, which caused severe ICP inside the porous support layer of the membrane hindering the flux through the membrane. The performance of all membranes was then tested when SAGD produced water was used as the feed solution. All the home made membranes had superior performance for water flux than the commercial membrane, with TFC3 achieving the highest water flux (about three times more than the commercial membrane). The rejection of TOC, silica and divalent ions for all the membranes was

more than 99%. Hence, the superiority of the home made TFC membrane both in term of water flux and high rejection was shown through this study.

5.2 Possible Future Directions

FO is still a burgeoning technology with significant improvements to be made for it to compete with other well established filtration processes. So here we highlight few recommendations and suggestions which can be carried out in the near future.

i. One of the most important aspects for the future advancement of FO is the design of suitable membranes which can achieve high flux while maintaining high rejection. The performance of the current commercial membranes is hindered due to the phenomena of ICP as explained in *Chapter 4*. High performance TFC films with ultra thin active layer were fabricated in this study. The performance of these membranes can further be improved by optimizing the support layer thickness of this membrane. Commercially available PES support which has a thickness of 140 μm was used as the support for these membranes. This thickness is still high as per supporting layer of a FO membrane. Reducing the thickness of the support layer will decrease the value of structural parameter diminishing the ICP effects inside the porous layer and improving the flux significantly. Another improvement which can be made to enhance flux through the membrane is increasing the hydrophilicity of the PES support. PES is known to be moderately hydrophobic [136,137] so blending certain additives such as polyethylene glycol (PEG) or polyvinyl pyrrolidinone (PVP) will increase the hydrophilicity of support facilitating water transport through the membrane [104].

ii. Following the successful application of FO in treatment of BFW, the next step can be using BBD as the feed solution. BBD is five times harsher than the BFW in terms of the amount of dissolved contaminants it has. This harsh quality of water cannot be treated with RO or NF process due to high propensity of membrane being fouled in these processes. But as it is well known that FO is less prone to fouling, as there is

no applied pressure acting on the membrane [77], so the possibility of membrane chocking with the deposition of contaminants is reduced to a great extent. Hence much harsher water with high amount TDS can be treated by a FO process.

iii. For the theoretical modeling of the FO, more investigations need to be made in finding appropriate methods to find the values of *K*. And as we have shown that the value of *K* depends on the values of mass transfer coefficient, so proper attention is needed to be devoted to find relations for mass transfer coefficient which would be applicable for an FO process. Better insight in the modeling process can be gained by using track-etched membranes, which have well defined straight cylindrical pores and hence the structural parameter of the membrane can be estimated. And once the structural parameter is known, the dependency of other parameters on the flow rates, draw solution concentration can be studied.

iv. The efficiency of a FO operation is highly dependent on the type of draw solution used. Ideally, a draw solution should be able to generate high osmotic pressure to achieve high water fluxes, it should be non-toxic and cheap [138]. But the most important criteria which need to be considered while making selection of a draw solutes is its recovery from the solution after a FO operation. The recovery of product water from the draw solution is the heart of a FO process and still a lot of research efforts are required to find a draw solution which can be regenerated by consuming minimum energy. One of the most popular draw solutions till date is the thermolytic draw solution of ammonium bicarbonate. The popularity of ammonium bicarbonate draw solution lies in the fact that it is highly soluble in water creating high osmotic force and when it is heated to around 60˚C the draw solutes decompose into ammonia and carbon dioxide gas. So with NH_3/CO_2 FO setup in operation, a portion of the diluted draw solution can be taken to stripping column where a temperature of around 60˚C can be used to decompose ammonium bicarbonate to NH_3 and CO_2 gas separating the draw solutes from the product water [37]. These gases can be condensed again to form ammonium bicarbonate when dissolved in

water at normal temperature to regenerate the draw solution. And for industrial application of this system, waste heat can be used to drive the thermal separation processes and the heat requirement of this hybrid system will be much less than that of the thermal separation processes because the heat supplied in FO will be used to vaporize the solutes from the solvent rather than vaporizing the solvent (water) to separate it from solutes [2,47].

And also, most of the FO applications and membrane characterizations in literature are based on using NaCl as the draw solution. So researchers need to focus on designing membranes and optimizing FO processes based on ammonium bicarbonate as a draw solution.

BIBLIOGRAPHY

[1] Facts on Water Resources, World Water. http://www.greenfacts.org/en/water-resources/.

[2] M. Elimelech, The global challenge for adequate and safe water, J. Water Supply Res. Technol. - AQUA. 55 (2006) 3–10.

[3] M. Shannon, P.W. Bohn, M. Elimelech, J.G. Georgiadis, B.J. Mariñas, A.M. Mayes, Science and technology for water purification in the coming decades., Nature. 452 (2008) 301–310.

[4] S. Zhao, L. Zou, C.Y. Tang, D. Mulcahy, Recent developments in forward osmosis: Opportunities and challenges, J. Memb. Sci. 396 (2012) 1–21.

[5] N.W. Arnell, Climate change and global water resources: SRES emissions and socio-economic scenarios, Glob. Environ. Chang. 14 (2004) 31–52.

[6] M. Elimelech, W. a Phillip, The future of seawater desalination: energy, technology, and the environment., Science. 333 (2011) 712–717.

[7] R.L. McGinnis, M. Elimelech, Global challenges in energy and water supply: The promise of engineered osmosis, Environ. Sci. Technol. 42 (2008) 8625–8629.

[8] P. Gleick, Water and Energy, Annu. Rev. Energy Environ. 19 (1994) 267–299.

[9] F. Birol, World Energy Outlook 2010, Int. Energy Agency. (2010) 738.

[10] S. Bhattacharjee, Oil Sands: A bridge between conventional petroleum and a sustainable energy future, in: Towar. Sustain. Clean Energy, 2011.

[11] R. Hill, Thermal In Situ Water Conservation Study, AI-EES and Jacobs Consultancy.

[12] S.E. Hrudey, Z. Xu, P. Gosselin, M.A. Naeth, A. Plourde, R. Therrien, et al., Environmental and Health Impacts of Canada ' s Oil Sands Industry, Engineering. (2010) 22.

[13] T. Pugsley, D. Pernitsky, J. Grundler, E.E. Johnsen, Fouling of heat transfer surfaces in a steam assisted gravity drainage (SAGD) in situ facility for the recovery of oil sands bitumen, 2013 (2013) 116–123.

[14] S. Wang, E. Axcell, R. Bosch, V. Little, Effects of Chemical Application on Antifouling in Steam-Assisted Gravity Drainage Operations, Energy & Fuels. 19 (2005) 1425–1429.

[15] D.W. Jennings, A. Shaikh, B. Petrolite, W. Airport, V. Boule, S. Land, Heat-Exchanger Deposition in an Inverted Steam-Assisted Gravity Drainage Operation . Part 1 . Inorganic and Organic Analyses of Deposit Samples, (2007) 176–184.

[16] A. Maiti, M. Sadrezadeh, S. Guha Thakurta, D.J. Pernitsky, S. Bhattacharjee, Characterization of boiler blowdown water from steam-assisted gravity drainage and silica-organic coprecipitation during acidification and ultrafiltration, Energy and Fuels. 26 (2012) 5604–5612.

[17] B.A.F.T.A. Krug, C.E.M.R. Canada, T.A. Krug, Oil removal from oilfield-produced water by cross flow ultrafiltration, (2000).

[18] A. Zaidi, K. Simms, S. Kak, The use of microultrafiltration for the removal of oil and suspended solids from oilfield brines, 25 (1992) 163–176.

[19] I.W. Cumming, R.G. Holdich, I.D. Smith, The rejection of oil using an asymmetric metal microfilter to separate an oil in water dispersion, Water Res. 33 (1999) 3587–3594.

[20] E. Gorouhi, M. Sadrzadeh, T. Mohammadi, Microfiltration of oily wastewater using PP hydrophobic membrane, Desalination. 200 (2006) 319–321.

[21] R.S. Faibish, Y. Cohen, Fouling and rejection behavior of ceramic and polymer-modified ceramic membranes for ultrafiltration of oil-in-water emulsions and microemulsions, Colloids Surfaces A Physicochem. Eng. Asp. 191 (2001) 27–40.

[22] T. Bilstad, E. Espedal, Membrane separation of produced water, Water Sci. Technol. 34 (1996) 239–246.

[23] Z. Wang, Y. Zhao, J. Wang, S. Wang, Studies on nanofiltration membrane fouling in the treatment of water solutions containing humic acids, Desalination. 178 (2005) 171–178.

[24] K.L. Jones, C.R. O'Melia, Protein and humic acid adsorption onto hydrophilic membrane surfaces: Effects of pH and ionic strength, J. Memb. Sci. 165 (2000) 31–46.

[25] C. A. Dyke, C.R. Bartels, Removal of organics from offshore produced waters using nanofiltration membrane technology, Environ. Prog. 9 (1990) 183–186.

[26] F.T. Tao, S. Curtice, R.D. Hobbs, J.L. Sides, J.D. Wieser, C. a Dyke, et al., Reverse osmosis process successfully converts oil field brine into freshwater, Oil&Gas J. 91 (1993) 88–91.

[27] M. Çakmakce, N. Kayaalp, I. Koyuncu, Desalination of produced water from oil production fields by membrane processes, Desalination. 222 (2008) 176–186.

[28] M. Sadrzadeh, J. Hajinasiri, S. Bhattacharjee, D. Pernitsky, Nanofiltration of oil sands boiler feed water: Effect of pH on water flux and organic and dissolved solid rejection, Sep. Purif. Technol. 141 (2015) 339–353.

[29] G.F. Doran, A. Alaska, K.L. Williams, B. Petroleum, J. a Drago, S. Sunny, et al., Pilot Study Results to Convert Oil Field Produced Water to Drinking Water or Reuse Quality, Int. Therm. Oper. Heavy Oil Symp. (1999).

[30] B.A. Braghetta, F. a Digiano, W.P.B. Member, Nanofiltration Of Natural Organic Matter: pH and Ionic Strenght Effects, (1994) 628–641.

[31] C. Murray-Gulde, J.E. Heatley, T. Karanfil, J.H. Rodgers, J.E. Myers, Performance of a hybrid reverse osmosis-constructed wetland treatment system for brackish oil field produced water, Water Res. 37 (2003) 705–713.

[32] A. Achilli, A.E. Childress, Pressure retarded osmosis: From the vision of Sidney Loeb to the first prototype installation - Review, Desalination. 261 (2010) 205–211.

[33] T. Cath, a Childress, M. Elimelech, Forward osmosis: Principles, applications, and recent developments, J. Memb. Sci. 281 (2006) 70–87.

[34] P. Venketeswari, O.S. Leong, N.H. Yong, Seawater desalination using forward osmosis process, J. Water Reuse Desalin. 4 (2014) 34.

[35] J.R. McCutcheon, R.L. McGinnis, M. Elimelech, A novel ammonia—carbon dioxide forward (direct) osmosis desalination process, Desalination. 174 (2005) 1–11.

[36] K.L. Lee, R.W. Baker, H.K. Lonsdale, Membranes for power generation by pressure-retarded osmosis, J. Memb. Sci. 8 (1981) 141–171.

[37] R.L. McGinnis, M. Elimelech, Energy requirements of ammonia–carbon dioxide forward osmosis desalination, Desalination. 207 (2007) 370–382.

[38] S. Lee, C. Boo, M. Elimelech, S. Hong, Comparison of fouling behavior in forward osmosis (FO) and reverse osmosis (RO), J. Memb. Sci. 365 (2010) 34–39.

[39] E. Cornelissen, D. Harmsen, K. Dekorte, C. Ruiken, J. Qin, H. Oo, et al., Membrane fouling and process performance of forward osmosis membranes on activated sludge, J. Memb. Sci. 319 (2008) 158–168.

[40] J.G. Wijmans, R.W. Baker, The solution-diffusion model: A review, J. Memb. Sci. 107 (1995) 1–21.

[41] R.W. Baker, Membrane Technology and Applications, Third Edit, Wiley, 2014.

[42] A. Fakhru'l-Razi, A. Pendashteh, L.C. Abdullah, D.R.A. Biak, S.S. Madaeni, Z.Z. Abidin, Review of technologies for oil and gas produced water treatment, J. Hazard. Mater. 170 (2009) 530–551.

[43] Y.S. Li, L. Yan, C.B. Xiang, L.J. Hong, Treatment of oily wastewater by organic-inorganic composite tubular ultrafiltration (UF) membranes, Desalination. 196 (2006) 76–83.

[44] B.D. Coday, P. Xu, E.G. Beaudry, J. Herron, K. Lampi, N.T. Hancock, et al., The sweet spot of forward osmosis: Treatment of produced water, drilling wastewater, and other complex and difficult liquid streams, Desalination. 333 (2014) 23–35.

[45] S. Mondal, S.R. Wickramasinghe, Produced water treatment by nanofiltration and reverse osmosis membranes, J. Memb. Sci. 322 (2008) 162–170.

[46] K. Lutchmiah, a R.D. Verliefde, K. Roest, L.C. Rietveld, E.R. Cornelissen, Forward osmosis for application in wastewater treatment: a review., Water Res. 58 (2014) 179–97.

[47] M.E. D.L Shaffer, J.R Werber, H.Jaramillo, S. Lin, Forward osmosis: Where are we now, Desalination. (2015) 271–284.

[48] S. Phuntsho, H.K. Shon, S. Hong, S. Lee, S. Vigneswaran, A novel low energy fertilizer driven forward osmosis desalination for direct fertigation: Evaluating the performance of fertilizer draw solutions, J. Memb. Sci. 375 (2011) 172–181.

[49] S. Phuntsho, H.K. Shon, T. Majeed, I. El Saliby, S. Vigneswaran, J. Kandasamy, et al., Blended fertilizers as draw solutions for fertilizer-drawn forward osmosis desalination, Environ. Sci. Technol. 46 (2012) 4567–4575.

[50] N.R. Hutchings, E.W. Appleton, R.A. Mcginnis, B.C. Services, Making High Quality Frac Water out of Oilfield Waste, (2010) 19–22.

[51] M. Xie, M. Zheng, P. Cooper, W.E. Price, L.D. Nghiem, M. Elimelech, Osmotic dilution for sustainable greenwall irrigation by liquid fertilizer: Performance and Implications, J. Memb. Sci. 494 (2015) 32–38.

[52] Q. Zhao, N. Chen, D. Zhao, X. Lu, Thermoresponsive magnetic nanoparticles for seawater desalination., ACS Appl. Mater. Interfaces. 5 (2013) 11453–61.

[53] R.J York, R.S Thiel, E.G Beaudry, Full-scale experience of direct osmosis concentration applied to leachate management, Proceedings of the 7th international waste mangement and landfill symposium, Cagliari, Sardinia, Italy (1999).

[54] R.W. Holloway, A.E. Childress, K.E. Dennett, T.Y. Cath, Forward osmosis for concentration of anaerobic digester centrate., Water Res. 41 (2007) 4005–14.

[55] S. Zhang, P. Wang, X. Fu, T.-S. Chung, Sustainable water recovery from oily wastewater via forward osmosis-membrane distillation (FO-MD)., Water Res. 52 (2014) 112–21.

[56] T.Y. Cath, N.T. Hancock, C.D. Lundin, C. Hoppe-Jones, J.E. Drewes, A multi-barrier osmotic dilution process for simultaneous desalination and purification of impaired water, J. Memb. Sci. 362 (2010) 417–426.

[57] K.L. Hickenbottom, N.T. Hancock, N.R. Hutchings, E.W. Appleton, E.G. Beaudry, P. Xu, et al., Forward osmosis treatment of drilling mud and fracturing wastewater from oil and gas operations, Desalination. 312 (2013) 60–66.

[58] B.D. Coday, N. Almaraz, T.Y. Cath, Forward osmosis desalination of oil and gas wastewater: Impacts of membrane selection and operating conditions on process performance, J. Memb. Sci. 488 (2015) 40–55.

[59] H. Peng, K. Volchek, M. MacKinnon, W.P. Wong, C.E. Brown, Application on to nanofiltration to water management options for oil sands operation, Desalination. 170 (2004) 137–150.

[60] Z. Wang, Y. Zhao, J. Wang, S. Wang, Studies on nanofiltration membrane fouling in the treatment of water solutions containing humic acids, Desalination. 178 (2005) 171–178.

[61] K.L. Jones, C.R. O'Melia, Protein and humic acid adsorption onto hydrophilic membrane surfaces: effects of pH and ionic strength, J. Memb. Sci. 165 (2000) 31–46.

[62] C. (United S. Tao, F.T.; Curtice, S.; Hobbs, R.D.; Sides, J.L.; Wieser, J.D. (Texaco Inc., Bellaire, TX (United States)); Dyke, C.A.; Tuohey, D. (Texaco Inc., Beacon,

NY (United States)); Pilger, P.F. (Texaco E and P Inc., Denver, Reverse osmosis process successfully converts oil field brine into freshwater, Oil Gas J. 91 (1993) 88–91.

[63] M. Çakmakce, N. Kayaalp, I. Koyuncu, Desalination of produced water from oil production fields by membrane processes, Desalination. 222 (2008) 176–186.

[64] N.C. Nguyen, S.-S. Chen, H.-Y. Yang, N.T. Hau, Application of forward osmosis on dewatering of high nutrient sludge., Bioresour. Technol. 132 (2013) 224–9.

[65] X. Zhang, Z. Ning, D.K. Wang, J.C. Diniz da Costa, Processing municipal wastewaters by forward osmosis using CTA membrane, J. Memb. Sci. 468 (2014) 269–275.

[66] K.B. Petrotos, H.N. Lazarides, Osmotic concentration of liquid foods, J. Food Eng. 49 (2001) 201–206.

[67] M.I. Dova, K.B. Petrotos, H.N. Lazarides, On the direct osmotic concentration of liquid foods. Part I: Impact of process parameters on process performance, J. Food Eng. 78 (2007) 422–430.

[68] W.H. Yang, Y.S. Tarng, Design optimization of cutting parameters for turning operations based on the Taguchi method, J. Mater. Process. Technol. 84 (1998) 122–129.

[69] M. Sadrzadeh, A. Razmi, T. Mohammadi, Separation of different ions from wastewater at various operating conditions using electrodialysis, Sep. Purif. Technol. 54 (2007) 147–156.

[70] S. Phuntsho, S. Vigneswaran, J. Kandasamy, S. Hong, S. Lee, H.K. Shon, Influence of temperature and temperature difference in the performance of forward osmosis desalination process, J. Memb. Sci. 415-416 (2012) 734–744.

[71] J.R. McCutcheon, M. Elimelech, Influence of concentrative and dilutive internal concentration polarization on flux behavior in forward osmosis, J. Memb. Sci. 284 (2006) 237–247.

[72] X. Jin, A. Jawor, S. Kim, E.M.V. Hoek, Effects of feed water temperature on separation performance and organic fouling of brackish water RO membranes, Desalination. 239 (2009) 346–359.

[73] P. Bacchin, D. Si-Hassen, V. Starov, M.. Clifton, P. Aimar, A unifying model for concentration polarization, gel-layer formation and particle deposition in cross-

flow membrane filtration of colloidal suspensions, Chem. Eng. Sci. 57 (2002) 77–91.

[74] T.H. Chong, F.S. Wong, A.G. Fane, Implications of critical flux and cake enhanced osmotic pressure (CEOP) on colloidal fouling in reverse osmosis: Experimental observations, J. Memb. Sci. 314 (2008) 101–111.

[75] Y. Xu, X. Peng, C.Y. Tang, Q.S. Fu, S. Nie, Effect of draw solution concentration and operating conditions on forward osmosis and pressure retarded osmosis performance in a spiral wound module, J. Memb. Sci. 348 (2010) 298–309.

[76] C. Suh, S. Lee, Modeling reverse draw solute flux in forward osmosis with external concentration polarization in both sides of the draw and feed solution, J. Memb. Sci. 427 (2013) 365–374.

[77] Y. Kim, M. Elimelech, H.K. Shon, S. Hong, Combined organic and colloidal fouling in forward osmosis: Fouling reversibility and the role of applied pressure, J. Memb. Sci. 460 (2014) 206–212.

[78] S. Guha Thakurta, A. Maiti, D.J. Pernitsky, S. Bhattacharjee, Dissolved Organic Matter in Steam Assisted Gravity Drainage Boiler Blow-Down Water, Energy & Fuels. 27 (2013) 3883–3890.

[79] T. Mohammadi, A. Moheb, M. Sadrzadeh, A. Razmi, Separation of copper ions by electrodialysis using Taguchi experimental design, Desalination. 169 (2004) 21–31.

[80] C. Klaysom, T.Y. Cath, T. Depuydt, I.F.J. Vankelecom, Forward and pressure retarded osmosis: potential solutions for global challenges in energy and water supply., Chem. Soc. Rev. 42 (2013) 6959–89.

[81] T.-S. Chung, X. Li, R.C. Ong, Q. Ge, H. Wang, G. Han, Emerging forward osmosis (FO) technologies and challenges ahead for clean water and clean energy applications, Curr. Opin. Chem. Eng. 1 (2012) 246–257.

[82] J.R. Mccutcheon, M. Elimelech, Modeling Water Flux in Forward Osmosis : Implications for Improved Membrane Design, 53 (2007) 1736–1744.

[83] G.D. Mehta, S. Loeb, Internal polarization in the porous substructure of a semipermeable membrane under pressure retarded osmosis, J. Memb. Sci. 4 (1978) 261–265.

[84] S. Loeb, L. Titelman, E. Korngold, J. Freiman, Effect of porous support fabric on osmosis through a Loeb-Sourirajan type asymmetric membrane, 129 (1997) 243–249.

[85] G.B. Berg, I.G. Racz, C. Smolders, Mass transfer coefficients ultrafiltration in cross-flow, J. Memb. Sci. 47 (1989) 25–51.

[86] B.H. V Gekas, Mass transfer in the membrane concentration polarization layer under turbulent cross flow: I. Critical literature review and adaptation of existing Sherwood correlations to membrane operations, J. Memb. Sci. 30 (1987) 153–170.

[87] G. Belfort, Fluid mechanics and cross-flow filtration: some thoughts, Desalination. 53 (1985) 57–79.

[88] C.H. Tan, H.Y. Ng, Modified models to predict flux behavior in forward osmosis in consideration of external and internal concentration polarizations, J. Memb. Sci. 324 (2008) 209–219.

[89] J.R. Welty, C.E. Wicks, R.E. Wilson, G. Rorrer, Fundamentals of Momentum, Heat, and Mass Transfer, 5th ed., John Wiley & Sons, Inc., 20078.

[90] C.P. Koutsou, S.G. Yiantsios, a. J. Karabelas, A numerical and experimental study of mass transfer in spacer-filled channels: Effects of spacer geometrical characteristics and Schmidt number, J. Memb. Sci. 326 (2009) 234–251.

[91] C. Rodrigues, M. Rodrigues, V. Semiao, V. Geraldes, Enhancement of mass transfer in spacer-filled channels under laminar regime by pulsatile flow, Chem. Eng. Sci. 123 (2015) 536–541.

[92] M. Hayatbakhsh, M. Sadrzadeh, D. Pernitsky, S. Bhattacharjee, J. Hajinasiri, Treatment of an *in situ* oil sands produced water by polymeric membranes, Desalin. Water Treat. (2015) 1–19.

[93] M.A. Al Mamun, M. Sadrzadeh, R. Chatterjee, S. Bhattacharjee, S. De, Colloidal fouling of nanofiltration membranes: A novel transient electrokinetic model and experimental study, Chem. Eng. Sci. 138 (2015) 153–163.

[94] S.S. Manickam, J.R. Mccutcheon, Model thin fi lm composite membranes for forward osmosis : Demonstrating the inaccuracy of existing structural parameter models, J. Memb. Sci. 483 (2015) 70–74.

[95] V. Lobo, Mutual diffusion coefficients in aqueous electrolyte solutions, Pure Appl. Chem. 65 (1993) 2613–2640.

[96] V. Vitagliano, P. a Lyons, Diffusion coefficients for aqueous solutions of sodium chloride and barium chloride, J. Am. Chem. Soc. 76 (1956) 1549–1552.

[97] W.A. Phillip, J.D. Schiffman, M. Elimelech, High Performance Thin-Film Membrane, 44 (2010) 3812–3818.

[98] K.Y.Wang, T.-S.Chung, G.Amy, Developing Thin-Film-Composite Forward Osmosis Membranes on the PES/SPSf Substrate Through Interfacial Polymerization, AIChE J. 58 (n.d.) 770–781.

[99] M. Qasim, N.A. Darwish, S. Sarp, N. Hilal, Water desalination by forward (direct) osmosis phenomenon: A comprehensive review, Desalination. 374 (2015) 47–69.

[100] J.T. Arena, B. McCloskey, B.D. Freeman, J.R. McCutcheon, Surface modification of thin film composite membrane support layers with polydopamine: Enabling use of reverse osmosis membranes in pressure retarded osmosis, J. Memb. Sci. 375 (2011) 55–62.

[101] C.H. Tan, H.Y. Ng, A novel hybrid forward osmosis - nanofiltration (FO-NF) process for seawater desalination: Draw solution selection and system configuration, Desalin. Water Treat. 13 (2010) 356–361.

[102] J. Ren, J.R. McCutcheon, A new commercial thin film composite membrane for forward osmosis, Desalination. 343 (2014) 187–193.

[103] W.J. Lau, A.F. Ismail, N. Misdan, M.A. Kassim, A recent progress in thin film composite membrane: A review, Desalination. 287 (2012) 190–199.

[104] R.J. Petersen, Composite reverse osmosis and nanofiltration membranes, J. Memb. Sci. 83 (1993) 81–150.

[105] J. Wei, C. Qiu, C.Y. Tang, R. Wang, A.G. Fane, Synthesis and characterization of flat-sheet thin film composite forward osmosis membranes, J. Memb. Sci. 372 (2011) 292–302.

[106] A. Tiraferri, N.Y. Yip, W. a. Phillip, J.D. Schiffman, M. Elimelech, Relating performance of thin-film composite forward osmosis membranes to support layer formation and structure, J. Memb. Sci. 367 (2011) 340–352.

[107] N. Widjojo, T.S. Chung, M. Weber, C. Maletzko, V. Warzelhan, The role of sulphonated polymer and macrovoid-free structure in the support layer for thin-film composite (TFC) forward osmosis (FO) membranes, J. Memb. Sci. 383 (2011) 214–223.

[108] Y. Yu, S. Seo, I.-C. Kim, S. Lee, Nanoporous polyethersulfone (PES) membrane with enhanced flux applied in forward osmosis process, J. Memb. Sci. 375 (2011) 63–68.

[109] L. Huang, J.R. Mccutcheon, Impact of support layer pore size on performance of thin fi lm composite membranes for forward osmosis, J. Memb. Sci. 483 (2015) 25–33.

[110] Y.H. Cho, J. Han, S. Han, M.D. Guiver, H.B. Park, Polyamide thin-film composite membranes based on carboxylated polysulfone microporous support membranes for forward osmosis, J. Memb. Sci. 445 (2013) 220–227.

[111] J.R. McCutcheon, M. Elimelech, Influence of membrane support layer hydrophobicity on water flux in osmotically driven membrane processes, J. Memb. Sci. 318 (2008) 458–466.

[112] M. Yasukawa, S. Mishima, M. Shibuya, D. Saeki, T. Takahashi, T. Miyoshi, et al., Preparation of a forward osmosis membrane using a highly porous polyketone microfiltration membrane as a novel support, J. Memb. Sci. 487 (2015) 51–59.

[113] G. Han, T.S. Chung, M. Toriida, S. Tamai, Thin-film composite forward osmosis membranes with novel hydrophilic supports for desalination, J. Memb. Sci. 423-424 (2012) 543–555.

[114] X. Li, K.Y. Wang, B. Helmer, T.S. Chung, Thin-film composite membranes and formation mechanism of thin-film layers on hydrophilic cellulose acetate propionate substrates for forward osmosis processes, Ind. Eng. Chem. Res. 51 (2012) 10039–10050.

[115] I.L. Alsvik, K.R. Zodrow, M. Elimelech, M.B. Hägg, Polyamide formation on a cellulose triacetate support for osmotic membranes: Effect of linking molecules on membrane performance, Desalination. 312 (2013) 2–9.

[116] N. Widjojo, T.-S. Chung, M. Weber, C. Maletzko, V. Warzelhan, A sulfonated polyphenylenesulfone (sPPSU) as the supporting substrate in thin film composite (TFC) membranes with enhanced performance for forward osmosis (FO), Chem. Eng. J. 220 (2013) 15–23.

[117] C. Klaysom, S. Hermans, A. Gahlaut, S. Van Craenenbroeck, I.F.J. Vankelecom, Polyamide/Polyacrylonitrile (PA/PAN) thin film composite osmosis membranes: Film optimization, characterization and performance evaluation, J. Memb. Sci. 445 (2013) 25–33.

[118] D. Emadzadeh, W.J. Lau, T. Matsuura, M. Rahbari-Sisakht, A.F. Ismail, A novel thin film composite forward osmosis membrane prepared from PSf–TiO2 nanocomposite substrate for water desalination, Chem. Eng. J. 237 (2014) 70–80.

[119] X. Song, Z. Liu, D.D. Sun, Nano gives the answer: breaking the bottleneck of internal concentration polarization with a nanofiber composite forward osmosis membrane for a high water production rate., Adv. Mater. 23 (2011) 3256–60.

[120] N.N. Bui, M.L. Lind, E.M. V Hoek, J.R. McCutcheon, Electrospun nanofiber supported thin film composite membranes for engineered osmosis, J. Memb. Sci. 385-386 (2011) 10–19.

[121] N.N. Bui, J.R. McCutcheon, Hydrophilic nanofibers as new supports for thin film composite membranes for engineered osmosis, Environ. Sci. Technol. 47 (2013) 1761–1769.

[122] M. Tian, C. Qiu, Y. Liao, S. Chou, R. Wang, Preparation of polyamide thin film composite forward osmosis membranes using electrospun polyvinylidene fluoride (PVDF) nanofibers as substrates, Sep. Purif. Technol. 118 (2013) 727–736.

[123] N.Y. Yip, A. Tiraferri, W.A. Phillip, J.D. Schiffman, L.A. Hoover, Y.C. Kim, et al., Thin-film composite pressure retarded osmosis membranes for sustainable power generation from salinity gradients., Environ. Sci. Technol. 45 (2011) 4360–9.

[124] A. Tiraferri, Y. Kang, E.P. Giannelis, M. Elimelech, Highly hydrophilic thin-film composite forward osmosis membranes functionalized with surface-tailored nanoparticles., ACS Appl. Mater. Interfaces. 4 (2012) 5044–53.

[125] N. Ma, J. Wei, R. Liao, C.Y. Tang, Zeolite-polyamide thin film nanocomposite membranes: Towards enhanced performance for forward osmosis, J. Memb. Sci. 405-406 (2012) 149–157.

[126] M. Amini, M. Jahanshahi, A. Rahimpour, Synthesis of novel thin film nanocomposite (TFN) forward osmosis membranes using functionalized multi-walled carbon nanotubes, J. Memb. Sci. 435 (2013) 233–241.

[127] N. Niksefat, M. Jahanshahi, A. Rahimpour, The effect of SiO2 nanoparticles on morphology and performance of thin film composite membranes for forward osmosis application, Desalination. 343 (2014) 140–146.

[128] A.K. Ghosh, B.-H. Jeong, X. Huang, E.M.V. Hoek, Impacts of reaction and curing conditions on polyamide composite reverse osmosis membrane properties, J. Memb. Sci. 311 (2008) 34–45.

[129] T.Y. Cath, M. Elimelech, J.R. McCutcheon, R.L. McGinnis, A. Achilli, D. Anastasio, et al., Standard Methodology for Evaluating Membrane Performance in Osmotically Driven Membrane Processes, Desalination. 312 (2013) 31–38. [130] M. Oldani, G. Schock, Characterization of ultrafiltration membranes by infrared spectroscopy, esca, and contact angle measurements, J. Memb. Sci. 43 (1989) 243–258.

[131] S. Belfer, Surface characterization by FTIR-ATR spectroscopy of polyethersulfone membranes-unmodified, modified and protein fouled, J. Memb. Sci. 172 (2000) 113–124.

[132] B.C. Smith, Infrared Spectral Interpretation: A Systematic Approach, CRC Press, 1998.

[133] C. Tang, Y. Kwon, J. Leckie, Probing the nano- and micro-scales of reverse osmosis membranes—A comprehensive characterization of physiochemical properties of uncoated and coated membranes by XPS, TEM, ATR-FTIR, and streaming potential measurements, J. Memb. Sci. 287 (2007) 146–156.

[134] Y. Song, F. Liu, B. Sun, Preparation, characterization, and application of thin film composite nanofiltration membranes, J. Appl. Polym. Sci. 95 (2005) 1251–1261.

[135] C.Y. Tang, Y.N. Kwon, J.O. Leckie, Effect of membrane chemistry and coating layer on physiochemical properties of thin film composite polyamide RO and NF membranes II. Membrane physiochemical properties and their dependence on polyamide and coating layers, Desalination. 242 (2009) 168–182.

[136] N. Arahman, Structure Change of Polyethersulfone Hollow Fiber Membrane Modified with Pluronic F127, Polyvinylpyrrolidone, and Tetronic 1307, Mater. Sci. Appl. 03 (2012) 72–77.

[137] J.R. McCutcheon, M. Elimelech, Influence of membrane support layer hydrophobicity on water flux in osmotically driven membrane processes, J. Memb. Sci. 318 (2008) 458–466.

[138] Q. Ge, M. Ling, T.-S. Chung, Draw solutions for forward osmosis processes: Developments, challenges, and prospects for the future, J. Memb. Sci. 442 (2013) 225–237.